Natural Resources Canada | Ressources naturelles Canada

GEOLOGICAL SURVEY OF CANADA
OPEN FILE 8814

Identification of regional structural corridors in the Montney play using trend surface analysis combined with geophysical imaging, British Columbia and Alberta

P. Wozniakowska, D.W. Eaton, C. Deblonde, A. Mort, and O.H. Ardakani

2021

Canada

GEOLOGICAL SURVEY OF CANADA
OPEN FILE 8814

Identification of regional structural corridors in the Montney play using trend surface analysis combined with geophysical imaging, British Columbia and Alberta

P. Wozniakowska[1], D.W. Eaton[1], C. Deblonde[2], A. Mort[2], and O.H. Ardakani[2,1]

[1]Department of Geoscience, University of Calgary, 2500 University Drive, Northwest, Calgary, Alberta
[2]Geological Survey of Canada, 3303-33rd Street N.W., Calgary, Alberta

2021

Permanent link: https://doi.org/10.4095/328850

This publication is available for free download through GEOSCAN (https://geoscan.nrcan.gc.ca/).

Recommended citation
Wozniakowska, P., Eaton, D.W., Deblonde, C., Mort, A., and Ardakani, O.H., 2021. Identification of regional structural corridors in the Montney play using trend surface analysis combined with geophysical imaging, British Columbia and Alberta; Geological Survey of Canada, Open File 8814, 1 .zip file. https://doi.org/10.4095/328850

Publications in this series have not been edited; they are released as submitted by the author.

Table of Contents

Abstract

The Western Canada Sedimentary Basin (WCSB) is a mature oil and gas basin with an extraordinary endowment of publicly accessible data. It contains structural elements of varying age, expressed as folding, faulting, and fracturing, which provide a record of tectonic activity during basin evolution. Knowledge of the structural architecture of the basin is crucial to understand its tectonic evolution; it also provides essential input for a range of geoscientific studies, including hydrogeology, geomechanics, and seismic risk analysis. This study focuses on an area defined by the subsurface extent of the Triassic Montney Formation, a region of the WCSB straddling the border between Alberta and British Columbia, and covering an area of approximately 130,000 km^2. In terms of regional structural elements, this area is roughly bisected by the east-west trending Dawson Creek Graben Complex (DCGC), which initially formed in the Late Carboniferous, and is bordered to the southwest by the Late Cretaceous - Paleocene Rocky Mountain thrust and fold belt (TFB). The structural geology of this region has been extensively studied, but structural elements compiled from previous studies exhibit inconsistencies arising from distinct subregions of investigation in previous studies, differences in the interpreted locations of faults, and inconsistent terminology. Moreover, in cases where faults are mapped based on unpublished proprietary data, many existing interpretations suffer from a lack of reproducibility. In this study, publicly accessible data - formation tops derived from well logs, LITHOPROBE seismic profiles and regional potential-field grids, are used to delineate regional structural elements. Where seismic profiles cross key structural features, these features are generally expressed as multi-stranded or *en echelon* faults and structurally-linked folds, rather than discrete faults. Furthermore, even in areas of relatively tight well control, individual fault structures cannot be discerned in a robust manner, because the spatial sampling is insufficient to resolve fault strands. We have therefore adopted a structural-corridor approach, where structural corridors are defined as laterally continuous trends, identified using geological trend surface analysis supported by geophysical data, that contain co-genetic faults and folds. Such structural trends have been documented in laboratory models of basement-involved faults and some types of structural corridors have been described as flower structures. The distinction between discrete faults and structural corridors is particularly important for induced-seismicity risk analysis, as the hazard posed by a single large structure differs from the hazard presented by a corridor of smaller pre-existing faults. We have implemented a workflow that uses trend surface analysis based on formation tops, with extensive quality control, combined with validation using available geophysical data. Seven formations are considered, from the Late Cretaceous Basal Fish Scale Zone (BFSZ) to the Wabamun Group. This approach helped to resolve the problem of limited spatial extent of available seismic data and provided a broader spatial coverage, enabling the investigation of structural trends throughout the entirety of the Montney play. In total, we identified 34 major structural corridors and number of smaller-scale structures, for which a GIS shapefile is included as a digital supplement to facilitate use of these features in other studies. Our study also outlines two buried regional foreland lobes of the Rocky Mountain TFB, both north and south of the DCGC.

Introduction

The Western Canada Sedimentary Basin (WCSB) contains structural elements, expressed as folding, faulting and fracturing, that record episodes of tectonic activity during the evolution of the basin. The WCSB is underlain by Precambrian crystalline basement, which formed through processes of tectonic assembly in the Paleoproterozoic (Ross et al., 1991; Ross et al., 1995), resulting in a mosaic of Archean and Proterozoic tectonic domains that are transected by lithosphere-scale sutures and continental-scale shear zones. The tectonic architecture of the crystalline basement provided a template for the development of younger depositional and structural features such as complex fault systems, extensive mountain belts and shear zones (Wright et al. 1994; Ross et al., 1991). Phanerozoic basin evolution of the WCSB was punctuated by relatively short-duration events that occurred within and adjacent to the basin, including Late Carboniferous collapse of the Peace River Arch to form the Dawson Creek Graben Complex (DCGC) and overlying Peace River Embayment (Barclay et al., 1990; Fox and Watson, 2019; O'Connell, 1990; Richards et al., 1990) and Late Cretaceous – Paleocene development of the Rocky Mountain TFB (Price, 1981; Pană and van der Pluijm, 2015; Skuce, 1996). Major shear zones expressed by significant horizontal displacement within crystalline rocks (Wright et al. 1994) are often indicative of basement reactivation (Pană, 2003). Some structural features are more subtle, such as inferred reactivation of basement faults that may be linked to the Middle Devonian Antler Orogeny (Root, 2001).

Understanding the distribution and architecture of structural elements in the WCSB is important for several reasons. Depending on their permeability characteristics, faults that extend from the basement into basin strata provide permeable conduits for crustal fluids or act as low-permeability fluid barriers (Smith, 1980). These features played a key role in hydrothermal fluids transport (Davies and Smith, 2006) and more complex geological processes, including mineral deposition and hydrothermal alteration processes (Hayba et al., 1985). For example, it has been proposed that the distribution of H_2S may be controlled by faults which facilitated upward migration of sulfate-bearing fluids from deeper sedimentary layers (Liseroudi et al., 2020). In addition, diagenetic processes, particularly dolomitization, are largely controlled by fluids and fault-controlled permeable pathways. Such pathways for crustal fluids have been invoked to explain pervasive dolomitization (Duggan et al. 2001; Davies and Smith, 2006; Green and Mountjoy, 2005). Many studies have suggested that basement structures influenced the nucleation and growth of Devonian reef complexes (Dix, 1993; Drivet and Mountjoy, 1997), which themselves profoundly influenced overlying strata through the process of tectonic inheritance. Finally, the development of unconventional resources such as tight oil and gas plays in the WCSB has relied on hydraulic fracturing, a technology that injects fluids under high pressure to create a fracture network as a means to enhance permeability of hydrocarbon-bearing rocks (Gale et al., 2014; Valkó, 2000). Together with the industry practice of large-volume disposal

of fluids, including co-produced formation brines and spent hydraulic fracturing fluids, fluid injection has resulted in a surge of induced seismicity (small-to-moderate earthquakes of anthropogenic origin) (Atkinson et al., 2016). Induced seismicity occurs on pre-existing faults that are critically stressed (Eaton, 2018; Fox and Watson, 2019; Chang and Segall, 2016). In principle, accurate and complete prior knowledge of the location and geometry of pre-existing faults can be used to inform hazard models in order to mitigate the risk of induced seismicity (e.g., Hennings et al., 2019).

This study focuses on the Montney resource play, which straddles the border between Alberta and BC in the WCSB (Fig. 1). Although permeable zones within the Montney region have been developed as conventional oil and gas pools for several decades, current development of the Montney Formation is focused on exploitation of its vast unconventional resource potential, estimated to contain 449 Tcf of marketable natural gas, 14,521 million barrels of marketable natural gas liquids, and 1,125 million barrels of marketable oil (National Energy Board, 2013). Previous studies suggest two-fold origin of the hydrocarbons in the Montney formation. According to the first model, the hydrocarbons within Montney are secondary bitumen that migrated through complex petro-structural pathways and accumulated within pore spaces (Wood et al., 2018). Alternative model is based on the concept of thermal maturation driven by the presence of the hydrothermal fluids that facilitate the process of hydrocarbon generation. Montney Formation is characterized by low permeabilities which hinder the transport of fluids, suggesting rather internal sources of hydrocarbons within the formation (Ducros et al., 2017; Romero-Sarmiento et al., 2016). Low-permeability reservoirs are often overpressured (*in situ* pore pressure above hydrostatic gradient ~10 kPa m^{-1}). Overpressure conditions in tight reservoirs develop during basin evolution, primarily due to inhibited water expulsion from the pores and/or hydrocarbon generation (Law & Dicknson, 1985; Hansom & Lee, 2005; Spencer, 1997). There is statistical evidence that overpressure of the Montney Formation is a risk factor for induced seismicity (Eaton and Schultz, 2018).

As the development of the Montney resource play has progressed over the past decade, it has become apparent that certain localized regions within the play are characterized by a relatively high geological susceptibility to induced seismicity during hydraulic fracturing operations (e.g., BC OGC 2014; Wozniakowska and Eaton, 2020). Areas of relatively high susceptibility to induced seismicity have, to date, largely been confined to northeastern BC, leading the BC Oil and Gas Commission to introduce regulatory measures to mitigate induced seismicity risks and improve the communication between industry, regulators, and local residents: North Peace Ground Motion Monitoring Area (NPGMMA) and the Kiskatinaw Seismic Monitoring and Mitigation Area (KSMMA) (according to *Guidance for Ground Motion Monitoring and Submission*). Measures include a requirement for careful planning of seismic monitoring and seismic risk

assessment, and deployment of accelerometers to monitor ground motions. In addition to ground motion monitoring, hydraulic fracturing and operations performed within KSMMA are regulated by a magnitude-based Traffic Light Protocol (TLP), which requires monitoring and reporting of earthquake magnitudes in real time, implementing seismic mitigation plans under 'yellow-light' conditions ($M_L > 2$[1]), or shut-in of operations under 'red-light' conditions ($M_L > 3$) (according to *ORDER 18-90-001*). In a report released in 2019, an expert panel commissioned by the Province of British Columbia concluded that the identification and mapping of critically stressed faults represents a significant current knowledge gap for induced seismicity risk mitigation (Allen et al., 2019).

Previous studies within the Montney play region have documented a significant number of blind faults – i.e., subsurface faults that lack any surface expression. Blind fault systems, especially connected with larger fault networks, have a potential to generate moderate natural earthquakes (Shaw and Suppe, 1996; Wolfe et al., 2019) or to act as permeable pathways for pore-pressure diffusion, causing hydraulic fracturing-induced seismicity at significant distances from the injection wells (Riazi and Eaton, 2020). Previous studies also document the existence of fault-related folds within Cretaceous formations, associated with upward-branching and lateral splays within blind faults (Hart et al., 2007). Examples of blind faults systems have been identified in multiple locations across the globe including US (Wolfe et al., 2019; Shaw and Shearer, 1999) and Europe (Butler, 1985; Vannoli et al., 2014).

Previous structural studies in the WCSB have focused primarily on individual faults, ostensibly treating these faults as isolated structural features. In contrast, analog models of basement-driven deformation within mechanically layered rocks reveal that this scenario rarely occurs. Previous analog studies show that basement-driven deformation typically leads to complex structures that include multiple generations of anastomosing, multi-strand faults and fault-propagation folds (e.g., Withjack & Callaway, 2000; Ackermann et al., 2001; Le Guerroué & Cobbold, 2006). In these complex structures, fracture systems develop in association with folds, as well as within damage zones that surround faults. Moreover, a multitude of field studies show that complex fault systems exhibit characteristic scaling behavior, such as power-law size distributions and empirical relationships between fault length and displacement (Cowie and Scholz, 1992; Dawers and Anders, 1995; Kim and Sanderson, 2005). Based on publicly available data, it is impractical to image and characterize such complex fault systems, yet it is inaccurate to reduce the description of structural elements to isolated faults. For example, while it is desirable, in principle, to use foreknowledge of pre-existing faults to forecast the a priori probability distribution for the maximum seismic moment of induced earthquakes, direct application of well-established earthquake scaling

[1] M_L denotes local earthquake magnitude

relationships (e.g., Kanamori and Anderson, 1975) to mapped faults (taking naïve fault length estimates derived from map length) leads to calculated seismic moments that are orders of magnitude larger than any observed induced earthquake. For these reasons, in this study we have adopted a different approach, through the identification and characterization of structural corridors rather than individual faults. We define a structural corridor as a laterally continuous spatial trend defined by a set of co-genetic structural features (faults and folds) inferred using geological and/or geophysical data. This approach simplifies the interpretive process of association of structures observed using different datasets; for example, trend surface residuals for specific formations, obtained using well control, provide broad spatial coverage that can be validated and refined where seismic data transect a structural corridor. This report provides an overview and analysis of the geophysical, geological, and geospatial datasets including 2D reflection seismic, geological formation tops, potential data, and previously mapped faults within the areal extent of the Montney formation and gives a summary of the structural elements that emerge from this comprehensive study.

Although the available well control provides extensive (albeit still incomplete) spatial coverage, even the relatively high density of well data that exists in the WCSB is insufficient to characterize structural features at scales (100s m) that are critical for induced seismicity risk analysis and understanding fluid systems. Resolution of structural features at this scale is possible using seismic-reflection data, but publicly accessible seismic data is sparse and often not utilized in past studies. Various structural studies have applied different local fault names to the same structures, which creates confusion when these studies are combined into an overall regional synthesis. Moreover, different previous studies contain small, but often significant at the scale of interest, differences in spatial positioning of important structural features, raising questions about the optimal approach for data integration, such as selecting one source or taking the average of several. Lineaments extracted from potential-field data have been used to infer potential faults (Edwards et al., 1998; Lyatsky et al., 2005), but regional signatures largely reflect basement structures and the influence of these features on Phanerozoic structural elements in the WCSB is often unclear. In this study, publicly accessible data - formation tops derived from well logs, LITHOPROBE seismic profiles and regional potential-field grids, are used to delineate regional structural elements. The structural framework developed herein can provide high-quality inputs for a number of geoscientific studies focusing on the fault distribution in the subsurface, including hydrological and geomechanical, and geochemical studies as well as seismic risk analysis (Bense et al., 2013, Fan et al., 2016; Liseroudi et al., 2020; Schoenball and Ellsworth, 2017).

Regional Setting

The Montney Formation was deposited along the western margin of Pangaea during the Early Triassic, over a period of about 5 million years (Gibson and Barclay, 1988; Edwards et al., 1994; Henderson et al., 2018). Lithofacies within the Montney Formation primarily consist of dolomitic siltstone, sandstone and bioclastic intervals, which were deposited within a shallow marine (shoreface through offshore) environment along a westwardly dipping ramp (Davies et al., 1997; Moslow and Davies, 1997; Crombez et al., 2016; Moslow et al., 2018; Davies et al., 2018). The formation is a westward thickening wedge that extends over more than 130,000 km^2 within the subsurface of west-central Alberta and north-eastern British Columbia, overlapping the Rocky Mountain TFB (Fig. 1) (Edwards et al., 1994; Davies et al., 1997). The maximum thickness of the Montney Formation is about 300 m, which is preserved within the major paleotopographic low of the Hudson Hope Embayment. The formation thins to a subcrop edge to the east (Davies et al., 2018; Rohais et al., 2018). Although the Montney Formation was once thought to have been deposited along a passive margin (e.g., Gibson and Barclay, 1988; Davies, 1997), recent studies have suggested an active margin setting during this time (Ferri and Zonneveld, 2008; Miall and Blakey, 2008; Beranek et al., 2010; Golding et al., 2016; Rohais et al., 2018; Morris et al., 2018). Pre-depositional, syn-depositional, and post-depositional activation and reactivation of structural features had impact on the distribution and preservation of sedimentological facies, and thereby influence the distribution of reservoir targets.

The Montney Formation is subdivided into the Lower, Middle and Upper members, which represent distinct depositional packages bounded by sequence boundaries that correspond to unconformities/correlative conformities that can be mapped basin-wide (Zonneveld and Moslow, 2018). The boundaries of these units correspond to major stage boundaries, with the Lower Montney being Griesbachian-Dienerian in age, the Middle Montney being Smithian, and the Upper Montney being Spathian (Henderson et al., 2018). Other members are more spatially and temporally isolated including the Calais Sandstone Member, Pocketknife Member, Anten Coquina Member, La Glace Sandstone Member and the Altarea Member (Zonneveld and Moslow, 2018). As a result of regulatory nomenclature, a slightly different terminology is used in Alberta and British Columbia to define the top of the Montney Formation and its subdivisions. In British Columbia, the Montney is subdivided into the Lower, Middle and Upper Montney, whereas in Alberta roughly correlative subdivisions are referred to as the Lower Montney, Upper Montney and Basal Doig siltstone, respectively (see Davies et al., 2018 and Zonneveld and Moslow, 2018 for further explanation and clarification). Herein, we will use the terminology of Lower, Middle and Upper Montney for its members. Visual presentation of Montney subdivision inn British Columbia and Alberta can be found in Appendix A (Fig. A1).

In a structural sense, the Montney play is characterized regionally by complex fault networks and major structural trends (Fig. 1) including the Dawson Creek Graben Complex (DCGC) and the Hay River Fault (HRF) Zone. Along its southwestern margin, the Montney play overlaps with the Rocky Mountain TFB. Although currently available compilations provide an extensive knowledge about the fault distributions in the area, there are arguably some areas where locations of faults are not well represented in the literature. For instance, outcrops of the eastern boundary of Late Cretaceous - Paleocene Cordilleran TFB compared with the previously mapped faults seem to overlap spatially in the northern part of Montney, which confirms that presence of the buried thrust belt (Riazi and Eaton, 2020). By analogy, similar tectonic patterns are expected in the vicinity of TFB in Alberta, yet to our knowledge equivalent structures are not present on published maps.

Figure 2 shows a map of seismicity in the study area, covering the period from January 2014 to December 2020. Earthquake activity is spatially clustered, rather than uniformly distributed, and apart from some seismicity clusters that are linked to known quarry blasts, the majority of events plotted in Figure 2 represent induced earthquakes (Schultz et al., 2020). Analogous to petroleum systems, the necessary conditions for the occurrence of felt induced earthquakes are: 1) a source of stress perturbation, such as a hydraulic fracturing program or a large-volume saltwater disposal well; b) a proximal, critically stressed fault with sufficient surface area to host a felt event (approximately $M > 2$, corresponding to fault dimensions of 100's m); 3) a pathway that connects the source to the fault (Eaton, 2018). Thus, observed clusters of induced seismicity highlight not only areas of industrial activity, but they also provide strong evidence for the presence of pre-existing faults within (but not necessarily limited to) the areas of the clusters. It is noteworthy that due to a combination of conditions, virtually all induced seismicity related to hydraulic fracturing in the Montney play occurs in northeastern BC rather than in Alberta (Wozniakowska and Eaton, 2020).

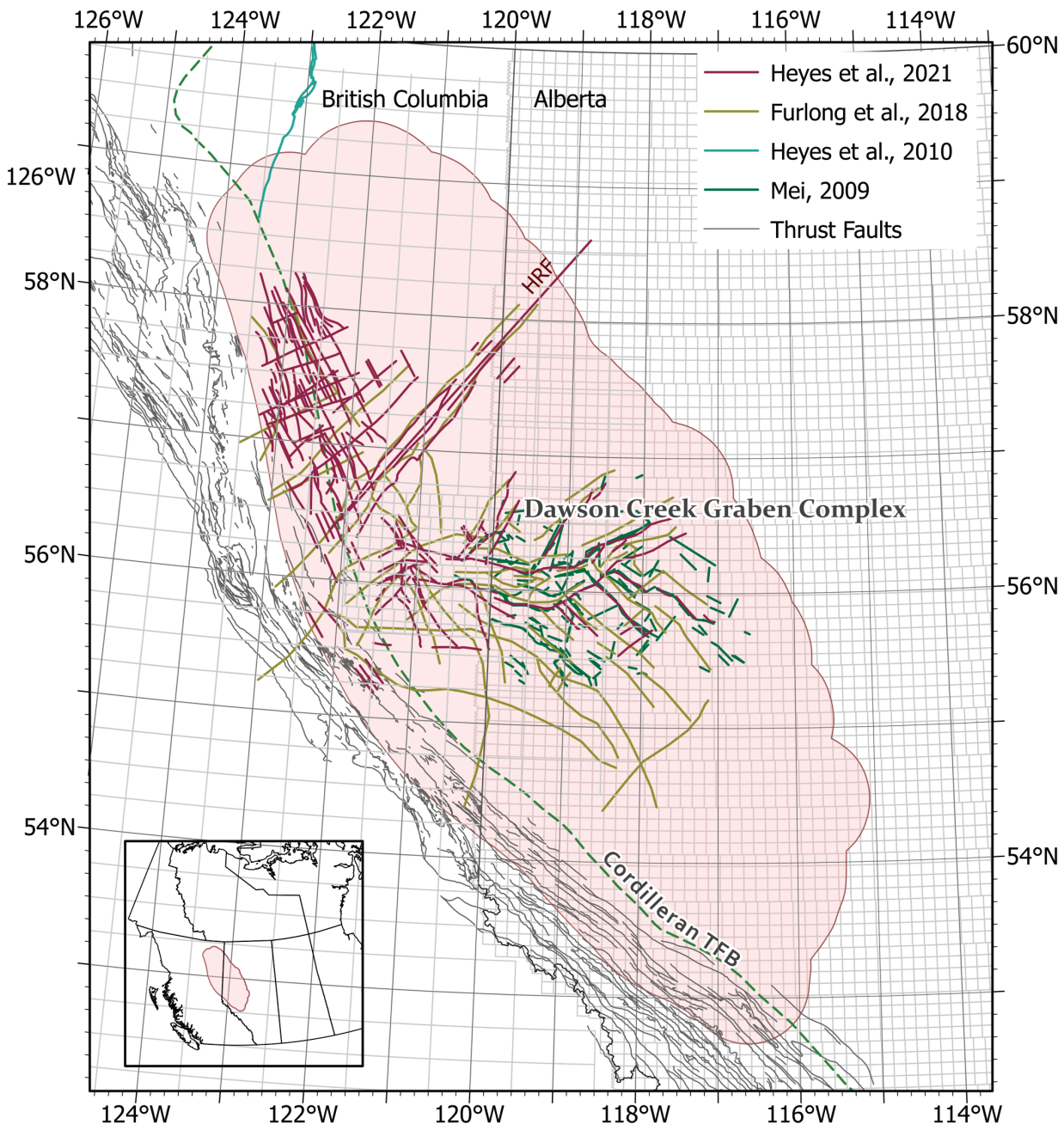

Fig. 1. Subsurface extent of the Montney Formation (shaded area), straddling the border between Alberta and BC. The eastern surface limit of the Late Cretaceous – Paleocene Cordilleran thrust and fold belt (TFB) is shown, along with published faults from previous studies that cover part of the Montney play (colored lines). There are three main areas of faulting; the northeast trending Hay River fault (HRF) represents a basement shear zone with an associated fault network delineated by oil and gas pools (e.g., Blueberry, Sikanni and Pocketknife) (Hayes et al., 2015; Hayes et al., 2021). To the northwest of the HRF, most of the faults are associated with a buried thrust belt (Riazi and Eaton, 2020). To the southeast of the HRF, most of the faults formed in the late Carboniferous as part of the Dawson Creek Graben Complex (Barclay et al., 1990). In areas of overlap between studies, previously mapped faults are in general agreement, but in detail, there are inconsistencies that hinder play-scale regional compilation.

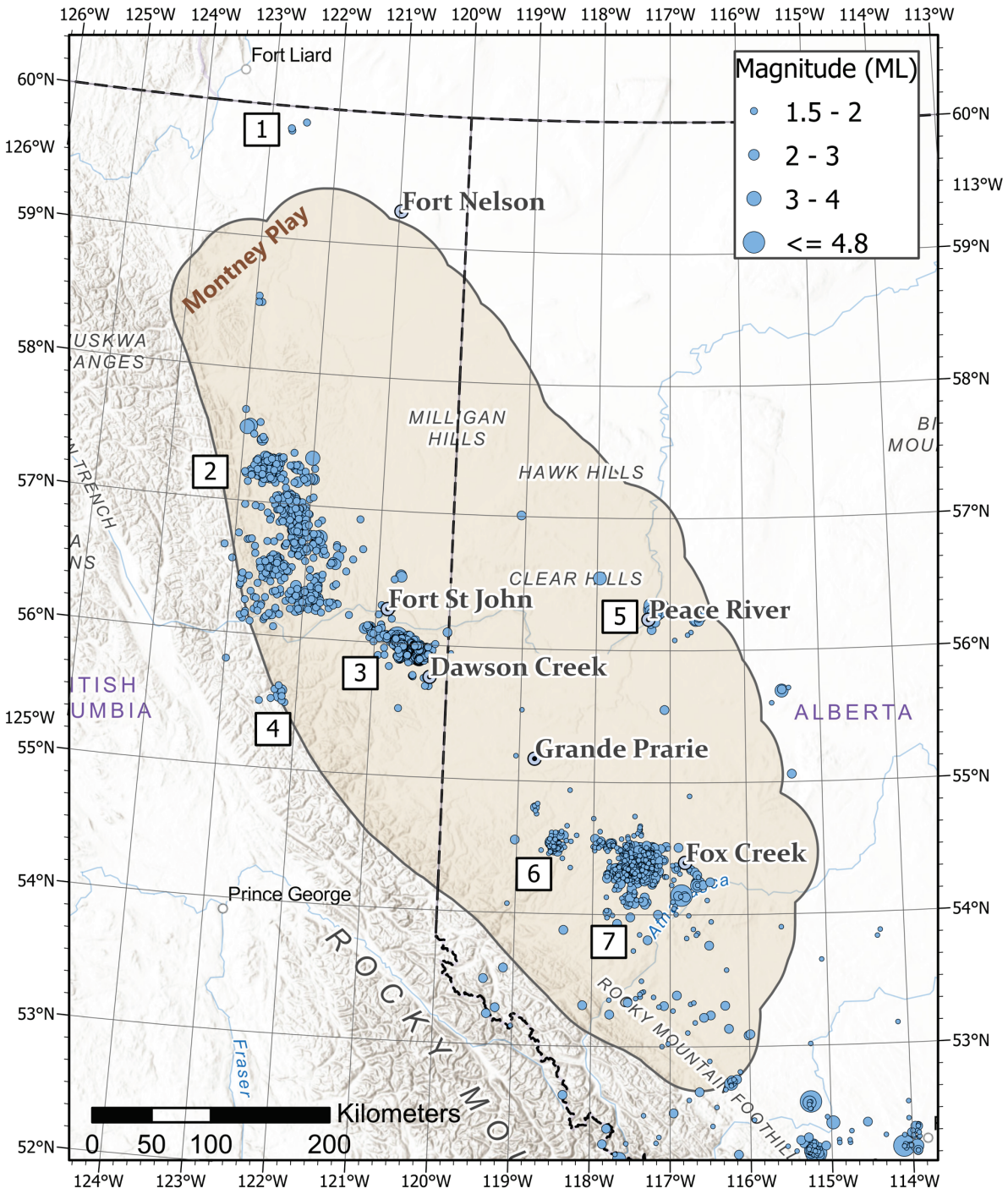

Fig. 2. (a) Map of seismicity (blue circles) in the Montney play (shaded region). Seismicity ($M_L \geq 1.5$) for the time period from January 2014 to December 2020 is indicated, compiled from earthquake catalogs provided by Alberta Energy Regulator and Natural Resources Canada. Seismicity clusters are numbered as follows: 1 = Horn River Basin (HRB), 2= northern Montney, 3 = Kiskatinaw, 4 = quarries, 5 = Peace River (enhanced oil recovery), 6 = Musreau Lake (wastewater disposal), and 7 = Fox Creek (Duvernay play). Seismicity clusters defined according to Schultz et al. (2020).

Methodology

The main steps in our workflow are summarized in the Figure 3.

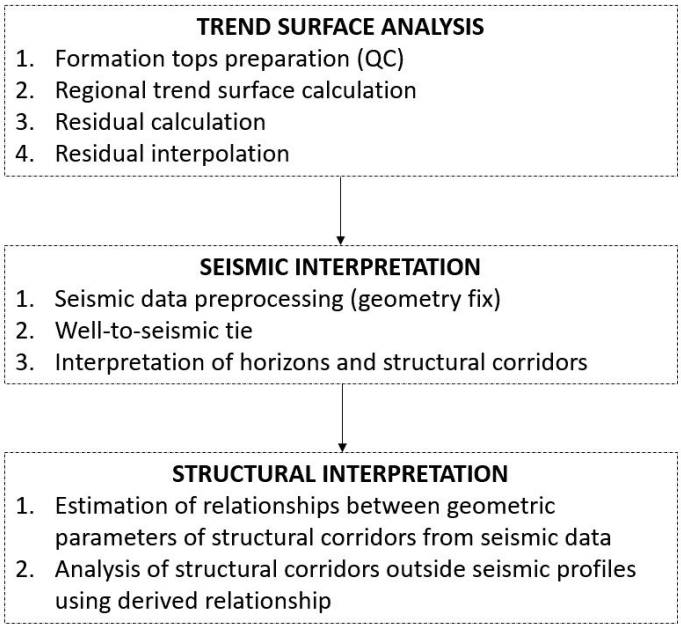

Fig. 3. Flow chart of the workflow used to process formation top data to identify faults using trend surface analysis and validate/characterize the results using regional reflection seismic data.

The first step of the analysis involves trend surface analysis applied to well log data, to identify major structural corridors using the residual mapping obtained from the geostatistical analysis of the formation-top picks. We analyzed 7 different geological formations from the period between Devonian to Cretaceous (Basal Fish Scale Zone, Bluesky, Halfway, Upper Montney, Belloy, Debolt, and Wabamun) to capture the evolution of the geological surfaces and allow for broader analysis of the tectonic activity and development of fault structures in time. Trend surface analysis consists of preprocessing, regional trend surface and residual calculations as well as the interpolation of residuals. Input data, detailed methodology as well as choice of parameters used are introduced in *Well log data and trend surface analysis* section.

The next step of the workflow was focused on the interpretation of the seismic data within the area of study. In addition to publicly available LITHOPROBE seismic profiles, we have analyzed one seismic line located within the KSMMA region near Fort St. John, BC. Preprocessing applied to the LITHOPROBE seismic profiles are described in Appendix A in the section *Seismic data – geometry preprocessing*.

In the last step, spatially limited information about subsurface structures from the trend surface analysis was complemented by seismic interpretation results. Specifically, seismic interpretation provided

information regarding the location of faults corresponding to the horizontal boundaries of structural corridors intersected by the seismic lines. Detailed location coordinates were subsequently used to calculate the width of the structures and compared with the corridors' length identified on the residual maps. Empirical relationship between length and width of the structures intersected by the seismic profiles were then used as a proxy to estimate geometric parameters for the remaining corridors, where seismic data are not available.

Geophysical Data

Potential-field Data

Potential-field data, including gravity and magnetic, can be used effectively to study structures underlying the sedimentary cover (Pilkington et al., 2000) as well as the tectonics and reactivation of basement faults (Ekpo et al., 2017). Within the study area, potential-field data were acquired from Natural Resources Canada's (NRCan) GEOSCAN online database, including total-field aeromagnetic data and isostatic gravity residual maps (Fig. 4). As described by Hope and Eaton (2002), regional magnetic anomaly data were prepared by NRCan by re-levelling various vintages of aeromagnetic surveys, with an average line spacing of 400m, followed by removal of the time-dependent International Geomagnetic Reference Field (IGRF). East of the Cordilleran TFB, magnetic anomalies predominantly reflect the configuration of tectonic domains in the crystalline basement, whereas in the interior of the Cordillera (in the SW corner of the map), short-wavelength anomalies reflect the distribution of shallow igneous intrusions in the Omineca belt. The transition between these domains is marked by a subdued magnetic signature that parallels the edge of the TFB; this subdued magnetic signature highlights areas where the ambient temperature within magnetic source regions exceeds the Curie temperature for magnetite (Bao et al., 2014). The isostatic residual gravity map was prepared by NRCan using data from gravity stations with an average spacing of 5-10 km, with tighter station spacing along LITHOPROBE seismic profiles (Hope and Eaton, 2002). The isostatic residual gravity anomaly accounts for varying station elevation (Bouguer and free-air corrections) as well as the predicted gravitational response based on deflection of the Moho assuming Airy isostatic compensation for surface topography (Goodacre et al., 1987). The isostatic anomalies therefore reflect density variations that cause mass excess or deficiency in the crust that deviates from the assumption of Airy isostacy. In the craton (east of the TFB), corresponding mass anomalies are supported by flexural strength of the lithosphere (Bao and Eaton, 2015) while to the west the observed isostatic gravity anomalies have a thermal origin (Hyndman and Currie, 2011).

Lineaments (sometimes subtle) can be extracted from potential-field maps using a variety of methods (e.g., Lyatsky et al., 2005). When lineaments are interpreted, it is important to be mindful of the fundamental

spatial resolution limits imposed by original acquisition of the data, as described above for the NRCan regional data used here. A multitude of conspicuous curvilinear features are evident, especially in the magnetic anomaly map, that are associated with tectonic domain boundaries in the crystalline basement. As described below, some curvilinear anomalies coincide with the Hay River, Dunvegan and Tangent faults (Fig. 4). Many other anomalous potential-field features, however, do not have any known association with faults that were active during the Phanerozoic. Therefore, to avoid potential false detections, the potential-field data are used in this study as a secondary source of information, rather than as primary datasets for fault identification.

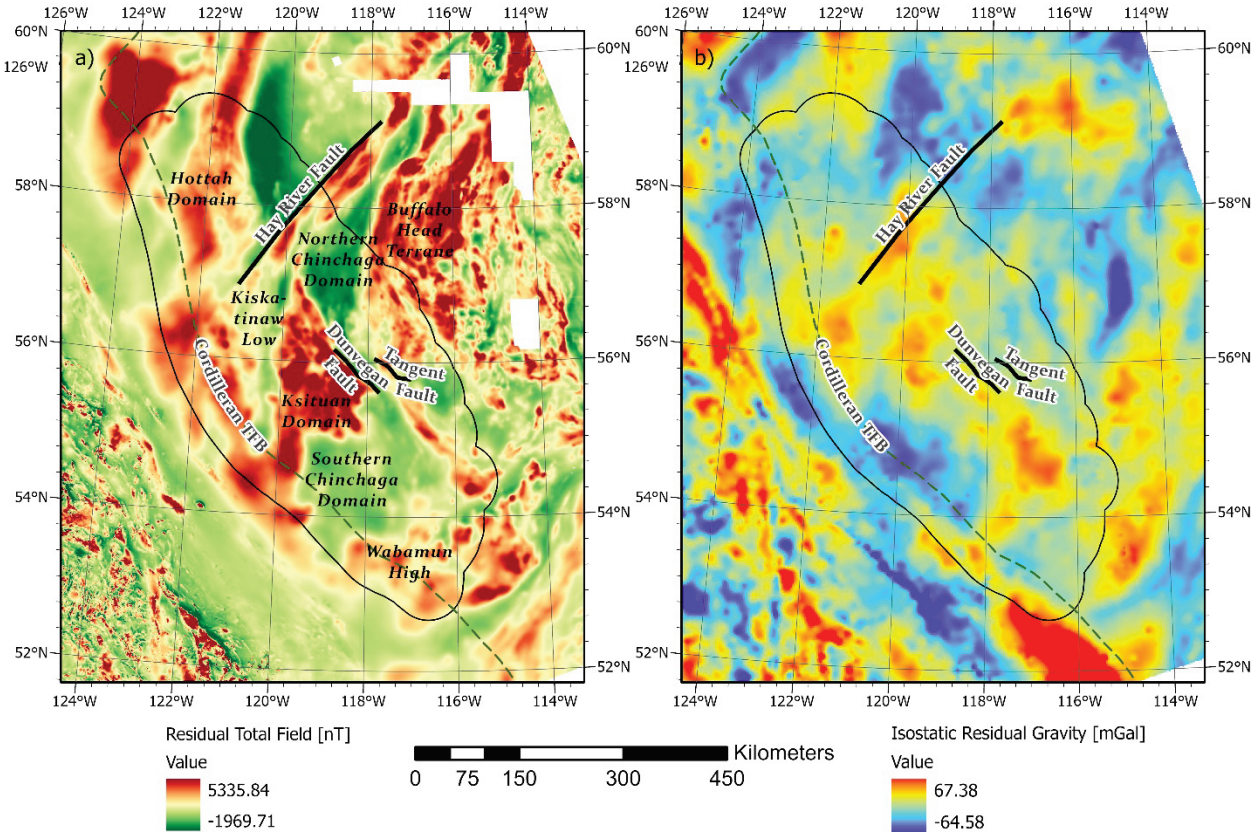

Fig. 4. a) Total-field magnetic anomaly map. Most of the faults shown in Fig. 1 have no clear potential-field expression, but three faults (Hay River, Dunvegan and Tangent faults) appear to have a prominent magnetic signature. Main tectonic domains within study area indicated. The eastern surface limit of the Late Cretaceous – Paleocene Cordilleran thrust and fold belt (TFB) is shown, for reference. b) Isostatic residual gravity anomaly map. Basement tectonic domains and the overall structural fabric of the TFB are evident, but apart from the Hay River, Dunvegan and Tangent faults, gravity anomalies at this scale show only a weak correlation with known faults from Fig. 1.

Seismic data and well ties

In 1994, Canada's LITHOPROBE program acquired 627 km of deep crustal seismic data within a crustal seismic transect called the Peace River Arch Industry Seismic Experiment (PRAISE) (Eaton et al., 1999;

Hope et al., 1999). The data, representing one of the primary sources of publicly available seismic data in western Canada, were acquired using Vibroseis sources, with a maximum two-way time of 18 s. This transect (Fig. 5) provides a piecewise continuous regional seismic profile that crosses many of the structural corridors of interest for this study, enabling seismic interpretation and characterization of the corridors. Migrated data were obtained from the Geological Survey of Canada (GSC) in SEGY format, along with survey files in SEGD format.

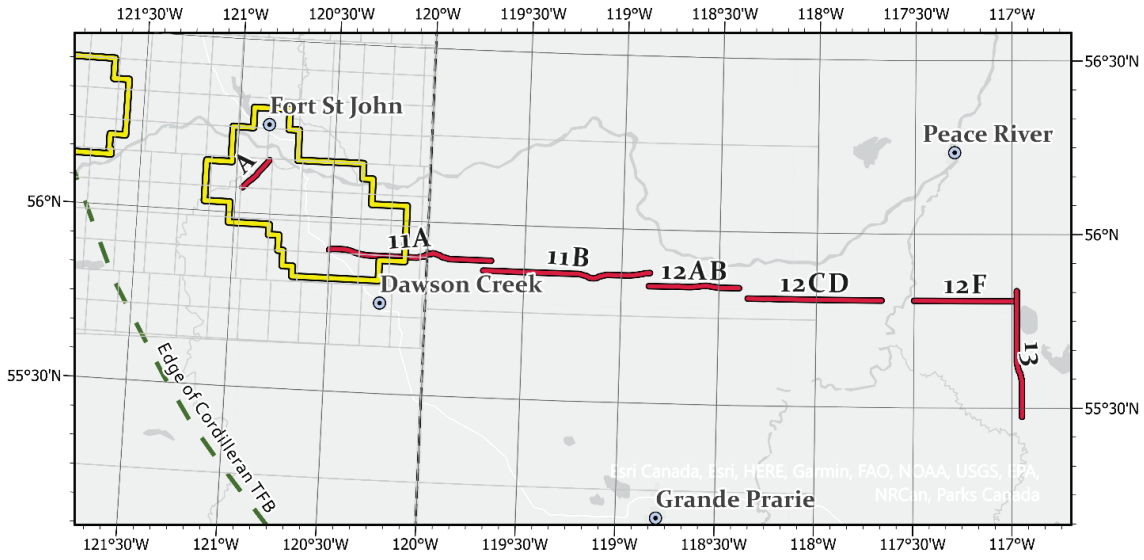

Fig. 5. Location of regional reflection seismic profiles used in the study, including LITHOPROBE PRAISE seismic lines 11A, 11B, 12AB, 12CD, 12F and 13 and a seismic line (A) provided for this study by Pulse Seismic Inc. The yellow outlines show induced seismicity monitoring and mitigation areas established by the BC Oil and Gas Commission.

Although the PRAISE data provide valuable information for this study, there are several limitations to consider. Due to the nature of the acquisition geometry, seismic-reflection profiles are not ideally suited for direct imaging of subvertical to vertical structures. In the case of a vertical strike-slip fault that laterally offsets reflectors in a horizontally stratified medium, the seismic expression of the fault may be subtle or non-existent, even if the lateral offset is significant. In addition, the ability to resolve small fault offsets is limited by the frequency content of the seismic data. For example, based on the (highly conservative) quarter-wavelength criterion (Sheriff, 1992), assuming a velocity of 4000 m/s and a dominant frequency of 25 Hz, the minimum resolvable fault offset is 40 m. Within a given structural corridor, this means that there are likely to be a large population of subseismic faults that have insufficient vertical offset to be detected. Various methods have been developed to account for small faults in reservoir analysis (Gauthier and Lake, 1993). In addition, immediately below the top of Precambrian basement the quality of LITHOPROBE seismic images is degraded due to the presence of multiple reflections that originate within the sedimentary basin

(Ross et al., 1995). This degraded zone, which extends for 1-2 s below the top of the basement, makes it difficult to discern reflections that may be associated with basement faults and shear zones.

It is important to note, that standard data processing procedures can impact the character of output seismic sections. For example, Automatic Gain Control (AGC) was applied during processing of the Lithoprobe data, to balance out amplitudes across the whole trace. This processing step is used to recover weaker, attenuated amplitudes and to improve the visibility of subtle structural features (Onajite, 2013; Westgate et al., 2021). Despite its benefit for enhancing weaker horizons that would otherwise be too weak to detect, AGC results in normalization of the amplitudes that prevents the extraction of true relative amplitudes after it is applied.

One of the crucial steps of the seismic interpretation was to perform a well tie. The purpose of well tie was to correlate the well log information to the 2D seismic lines. Specifically, a sonic log was used to determine the time-depth relationship, which was followed by the calculation of synthetic reflection coefficients from sonic and density logs. Reflection coefficients were convolved with the zero-phase wavelet extracted from the seismic lines within 1000-3000ms with wavelength of and taper length set to 120ms and 20ms respectively. The synthetic seismogram was subsequently fit to seismic data by shifting the seismic trace up or down or applying a small degree of stretching within specific depth intervals to achieve a satisfactory match. Seismic well-ties were performed using four representative wells located within 5 km of the LITHOPROBE seismic profiles: 100/13-02-080-15W6/00 (Line 11a), 100/16-29-079-10W6/00 (Line 11b), 100/16-33-078-25W5/00 (Line 12ab), 100-13-020-080-15W6/00 (Line 12F), 100/14-21-074-19W5/00 (Line 13). An example of a seismic-well tie performed for the well 100/10-02-079-22W5/00 is presented in the Figure 6.

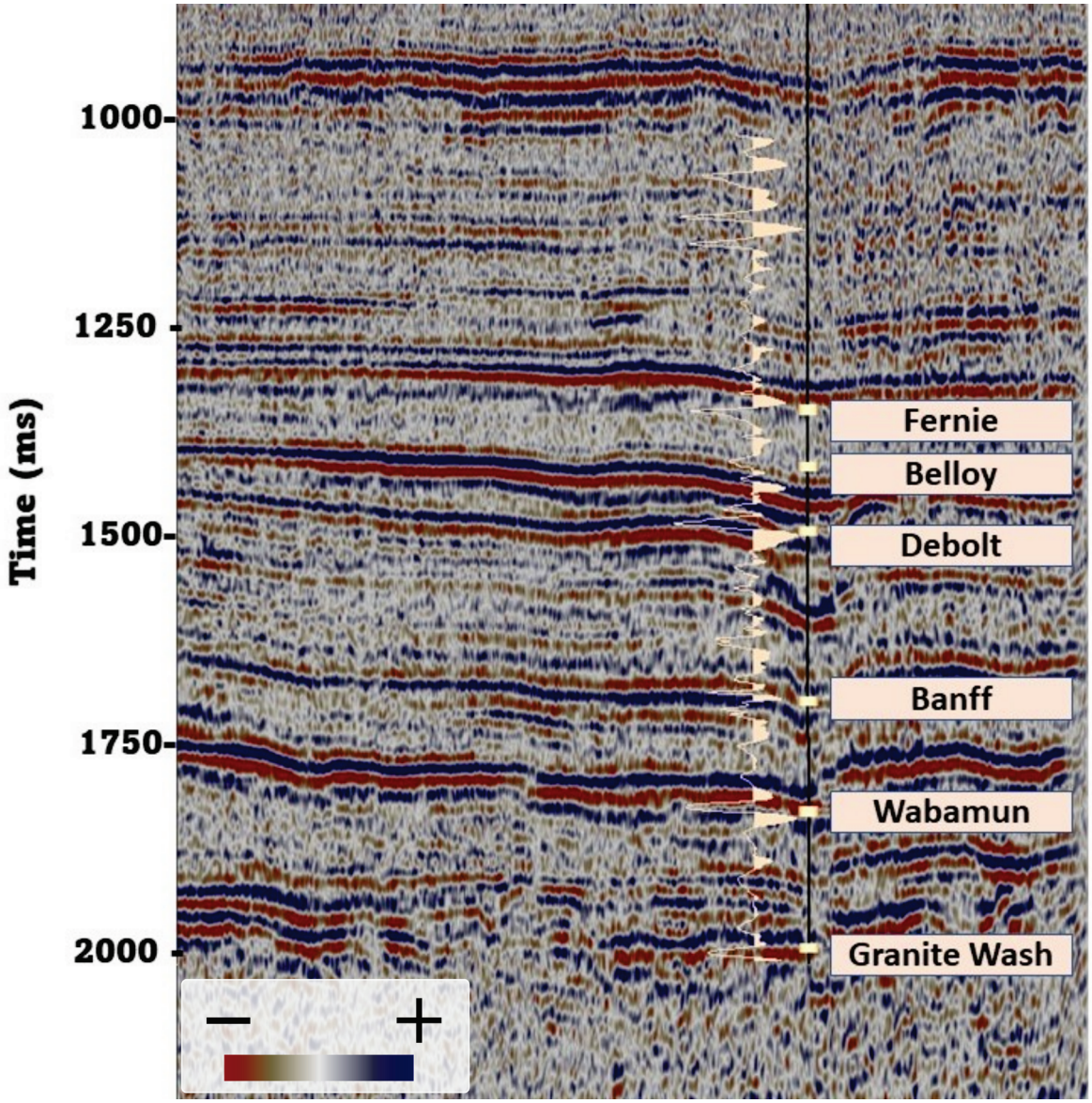

Fig. 6. Example seismic-well tie performed for the LITHOPROBE line 12F and well 100/10-02-079-22W5/00. Black line represents the synthetic seismogram fit to seismic data with correlation coefficient of 0.63 in the interval between Fernie and Granite Wash horizons which represent the strongest reflectors within the analyzed depth range. Red and blue colors on the seismic section corresponds to negative and positive relative amplitude, respectively.

Well log data and trend surface analysis

The availability of formation tops picked in oil and gas wells drilled throughout the study area provides critical, spatially extensive geological data for interpretation of fault systems. Fault interpretation is facilitated in this study by constructing a residual surface, obtained by interpolating the observed picks and subtraction it from a trend surface that provides a smooth fit to the formation-top surface. The method is based on a previously developed workflow that uses a geostatistical approach (Mei, 2009). The concept is

simple: an abrupt lateral change in surface elevation due to vertical fault offset will produce a paired anomaly, with a negative residual in the hanging wall and a positive residual in the footwall. Folds are also considered in our interpretation of structural corridors. In the case of a fold with wavelength that is small compared with the spatial smoothing, the residual anomaly is not necessarily a positive-negative pair; in general, an antiform will produce a negative residual and a synform will produce a positive residual. Where a significant paired residual anomaly is evident, the location of the corresponding fault is approximated by the zero crossing of the residual surface, while the apparent local vertical fault throw is given by the elevation difference between the positive and negative residual anomalies, measured perpendicular to the anomaly strike direction. As elaborated below, the apparent vertical throw underestimates the actual throw due to some of the structural relief being taken up in the trend surface. Similar to the limitations of seismic interpretation discussed above, this method is not well suited to identification of faults with strike-slip offset, unless some vertical offset in formation tops occurs due to regional dip and/or mixed-mode (oblique) fault slip. It is also important to recognize that the choice of smoothing parameters has an effect on the estimated fault offset, leading to uncertainty in the estimated fault throw. In general, the actual throw is greater than, or equal to, the apparent fault throw estimated using this approach. In addition, well spacing has an impact; for example, if two or more faults are located between two wells, these will be expressed in this analysis as a single effective fault.

This approach yields important constraints on fault geometry and the timing of deformation. In particular, a measured fault displacement implies net deformation that postdates deposition of the formation in question, or, in the special case of growth faults, deformation that is synchronous with deposition. Based on this principle, in the case of a difference in the estimated throw on a fault that intersects two formations, the younger formation is expected to show less net displacement, since the net displacement occurred within a shorter period of time. However, it is also possible for a younger formation to show deformation that is not expressed on a deeper formation, if the fault does not intersect the deeper formation, e.g., if it soles into a shallower detachment. Folds also play a significant role in structural corridors; as discussed below, seismic evidence shows that some faults terminate up-dip into (fault-propagation) folds that formed at the same time as the fault. Finally, it is important to recognize that deformation likely occurred within discrete episodes of tectonic activity, rather than continuously throughout the evolution of the basin. Recorded fault offsets thus reflect net deformation that accumulated, considering the entire tectonic history of the fault.

The geoSCOUT database provided the primary source of data for well tops. This database is derived from reports submitted by oil and gas operators, wherein formation tops are necessarily picked by different people, with varying experience and interpretive biases. Consequently, it is important to ensure accuracy of formation picks and remove outliers, to the extent that this is practical given > 100,000 data points. In

this study, a two-stage quality-control approach was used. In the first stage, wells with incorrect values (extremely high or extremely low) relative to surrounding wells were removed from the analysis. In the next stage, duplicate information resulting from multiple wells or data entry error were investigated to remove incorrect entries. In cases where the correct entry was unclear, multiple values at the same location were averaged.

The following formations tops are considered in this study:

- Basal Fish Scale Zone (Cretaceous)
- Bluesky (Cretaceous)
- Halfway (Triassic)
- Upper Montney (Triassic)
- Belloy (Permian)
- Debolt (Carboniferous)
- Wabamun (Devonian)

The selection of formation tops was based on the availability and inferred reliability of the picks in the geoSCOUT database. The formations were also chosen to enable analysis of episodic fault reactivation of the history of the WCSB. Some formation tops would have been desirable to include (e.g., top of Precambrian basement), but the available picks were too sparse. Where possible, the same formations chosen for trend surface analysis were also used for the seismic interpretation.

After completion of quality control, the trend surface analysis method was implemented using the Geostatistical Wizard Toolbox included in ArcGIS Pro Software. The following steps were used:

1. *Local Polynomial Regression*

   Following Mei (2009), for each formation top a 3rd order polynomial surface was fit to the data within user-defined overlapping neighborhoods. The trend surface was interpolated using an exponential kernel with minimum of 10 and maximum of 1000 neighboring points, a search circle size of 45km, and 4 search sectors within 45° offset.

2. *Residual calculation*

   A raw residual point set was determined by subtracting formation tops from the 3rd-order trend surface (Fig. 7). Simple kriging was applied to the residual data, after the following preprocessing steps: (i) normal-score transformation with the multiplicate skewing approximation to account for non-normal distribution of residual values; (ii) declustering using a cell size of 1000m, based on the average minimal distance in less populated areas according to histogram of the inter-well distances.

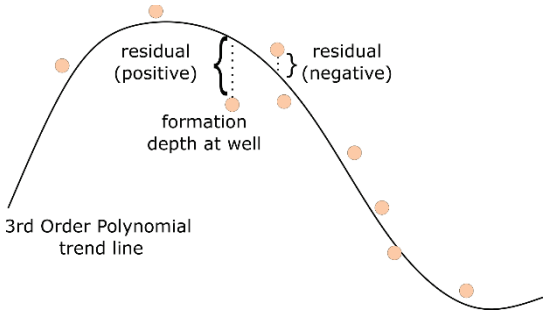

Fig. 7. Graphical representation of 3rd order residual calculation. Black line corresponds to the 3rd Order Polynomial trend line calculated using Local Polynomial Interpolation method. Residuals are calculated by extracting the value of the formation depth picked by a geologist at given well from the value corresponding to the Regional Trend Surface at the location of the well.

3. *Rasterization of residual maps*

   Georeferenced raster images for each residual surface were created using the ArcGIS kriged layer to raster function, with a 250m × 250m cell. The grey scale range for each residual map was clipped by discarding 0.5% of the lowest and highest values of the residuals. In practice, this approach removed the most extreme, potentially incorrect estimates and yields a smoother residual surface.

The choices of parameters listed above are somewhat subjective. There is considerable flexibility in the application of the trend surface residual approach, but parameter choices require careful testing based on the distribution of the data. Consistent with Mei (2009), parameters for each formation were optimized by visually fitting the semivariogram to the input data using 12 lags and lag size of 1100m and correcting for anisotropy according to the semivariogram, with average direction of major range of 150 degrees. Anisotropy ranges were specified on semivariogram maps individually for each formation, with minimum values between 6 to 8 km and maximum between 10 to 12 km. Remaining parameters including sill and nugget were selected automatically by the software to minimize the RMS misfit, given the assigned parameters described above.

Results

Well log data and trend surface analysis

Figure 8 shows grayscale images of residual maps for four of the formations listed above (corresponding maps for other formations are given in Appendix A). The spatial resolution, and therefore the ability to resolve short-wavelength structure, depends on the number of picks available. The best spatial resolution is provided by the Basal Fish Scale Zone (BSFZ), for which 104,073 wells were available to construct the residual map, compared with about 20,000 wells for the other formations. The spatial extent for each map

is limited to the region of available well data, and the extreme values of the grayscale depend on the minimum and maximum residual values.

In the case of the oldest units shown in Figure 8 (Wabamun and Debolt), the east-west trending Dawson Creek Graben Complex (DCGC) is conspicuous, near 56º N. This structural belt has a total length of approximately 250 km and consists of a series of grabens, the largest of which is the Fort St. John graben (FSJG). To the north and east, this complex contains major, oblique-trending satellite grabens including the Hines Creek, Dunvegan, Tangent and Boundary Lake grabens. The DCGC formed in late Carboniferous time due to collapse of the underlying Peace River Arch (Barclay et al., 1990; Eaton et al., 1999). Although the residual maps indicate a maximum apparent throw of just over 76m, this value significantly underestimates the actual vertical throw since, as noted above, part of the structural relief is taken up by the trend surface. To the west, the DCGC extends into the disturbed belt, although in these maps its western limit is obscure due to lack of well control at the Debolt and Wabamun levels. In the case of the Wabamun residual map, several isolated high features are well constrained by drilling and lie above major reefs (atolls) within the underlying Leduc and Swan Hills formations. These residual highs may represent the effects of differential compaction, as underlying off-reef strata (e.g., Ireton shale) are more compacted than the Leduc reefs (O'Connor and Gretener, 1974). Despite careful efforts for quality control, however, there are a few isolated features ("bulls eye" anomalies) in both the Debolt and Wabamun maps that are inferred to represent data outliers, not true structural features. In general, structural corridors correlate with anomalies that exhibit a coherent trend.

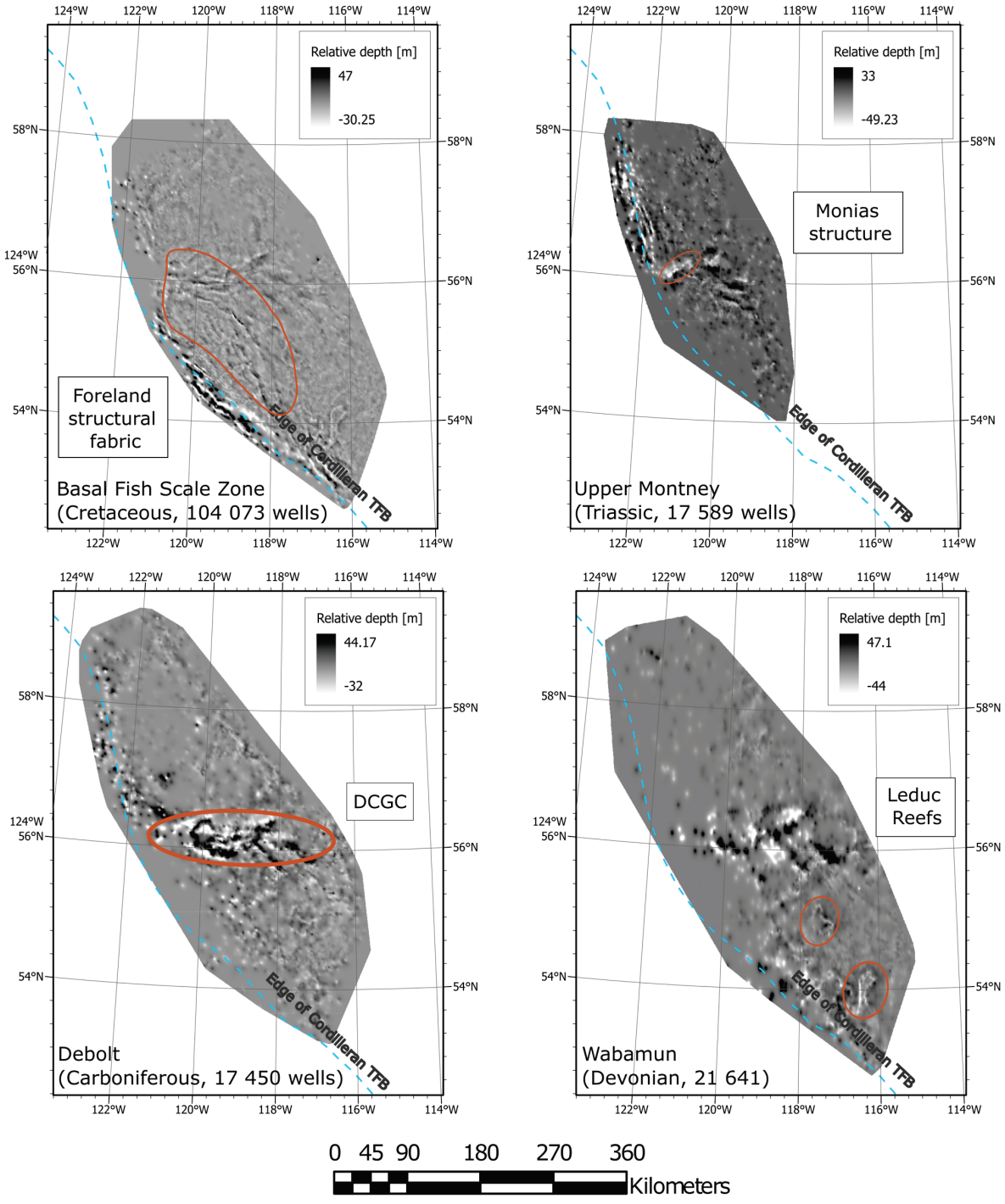

Fig. 8. Residual maps of Basal Fish Scale Zone, Upper Montney, Debolt and Wabamun tops. Coherent trends in the maps are indicative of structural corridors (faults and folds). For reference, the eastern edge of the Cordilleran thrust and fold belt (TFB) is indicated by the dashed blue line. Major structural trends expressed on the residual maps are outlined in red. For each unit, the age and number of wells used for residual calculation are indicated in the lower left of the map.

In the case of the Upper Montney residual map (Fig. 8), some features in the DCGC can be discerned, although it is clear that only some parts of the DCGC were active during and/or after deposition of the Upper Montney. One example is the northeast trending, Monias structure, which appears to truncate the east-west trending FSJG. In the northwestern part of the Montney play, available well control highlights structural features that are part of the Cordilleran TFB. These features formed in the Late Cretaceous – Paleocene and extend some distance to the east of the edge of the TFB, forming buried lobes of the thrust belt (Fig. 1). The Debolt Formation also shows evidence for thrust features in the northwestern Montney play, but these are absent for the Wabamun (Fig. 8). As noted by Riazi and Eaton (2020), the Banff Formation, which lies above the Wabamun, forms a regional décollement surface for the buried thrust belt; hence, in this area the Wabamun Formation is autochthonous and was not directly impacted by Cordilleran TFB structural shortening.

The BFSZ also shows evidence of deformation that appears to be associated with reactivation of certain parts of the DCGC, especially on the Alberta side of the provincial border (east of 120ºW). In particular, the southern flank of the underlying DCGC, near the border with BC, as well as satellite grabens to the east, show evidence for reactivation. Thrusting within the Cordilleran TFB in the southern part of the Montney play is also conspicuous, but the northern part of the thrust belt is more subtly expressed than in the Upper Montney (Fig. 8). Due to the abundance of well control, the BFS clearly records a number of short-wavelength features with high fidelity. For example, the Leduc reef structures that are visible in the Wabamun map area also apparent in the BFS residual, indicating that the effects of differential compaction extended high up in the stratigraphic succession. There is also a subtle but coherent anomaly trend in the BFSZ residual that lies above the Hay River fault. Additionally, in the foreland east of the TFB and south of the DCGC, a well-defined structural fabric is expressed in the map, sub-parallel to the eastern edge of the TFB. Notably, this structural fabric extends into the region of induced seismicity south of Fort St. John, as well as a recently active cluster of induced seismicity near Musreau Lake (Fig. 2). This BFSZ structural fabric in the southern Montney is not apparent in deeper residual maps, possibly because there is insufficient well control at deeper levels to delineate these features, based on the method used here.

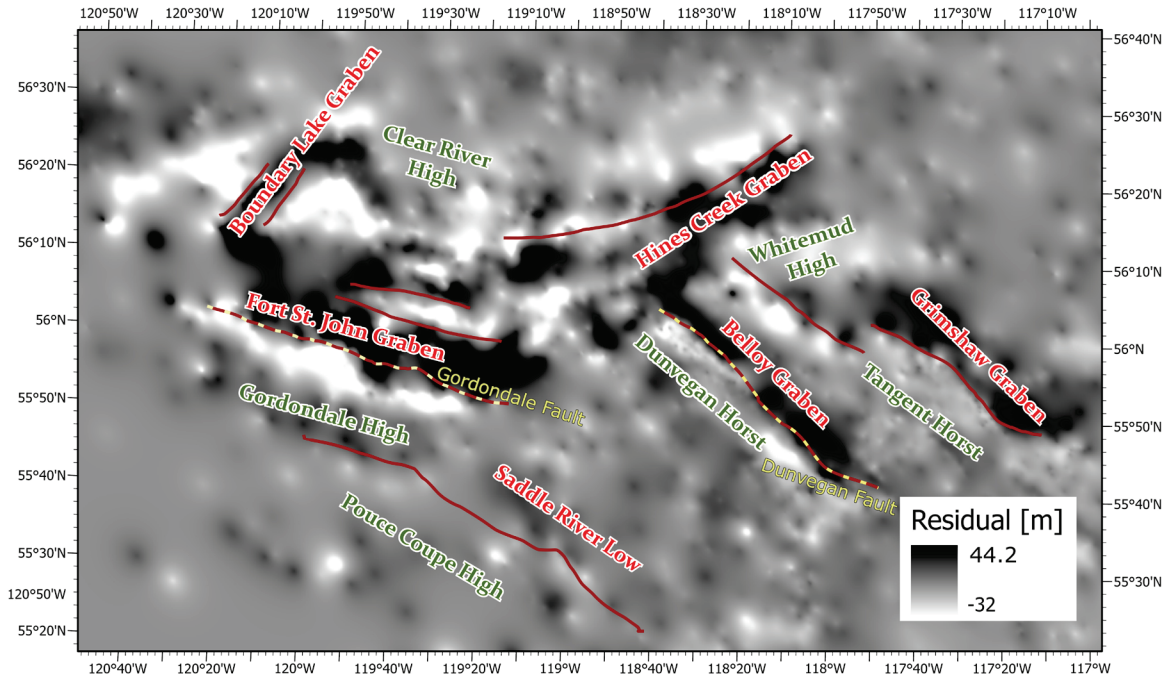

Fig. 9. Enlargement of the Debolt residual map in the vicinity of the Dawson Creek Graben Complex (DCGC), showing the primary graben structure (Fort St. John graben, FSJG) and satellite grabens to the north and east. Dip slip fault zones are indicated by a paired positive-negative anomaly, as indicated by the red lines. Gordondale and Dunvegan faults are indicated by the red and yellow lines.

An enlargement of the Debolt residual map in the DCGC is presented in Fig. 9. As elaborated above, normal faults appear as a positive-negative paired anomaly. Furthermore, multiple, *en echelon* faults tend to be grouped together, thus limiting resolution of internal details within structure corridors. Some features, such as the southern bounding fault of the Fort St. JG (the Gordondale fault), and the Dunvegan fault, exhibit a high degree of lateral continuity, whereas other features such as the Hines Creek graben appear to be more discontinuous**.** Similar trends can be observed for the Basal Fish Scale Zone (Fig. 10) and Upper Montney (Fig. 11) residual maps. Our method for obtaining these residuals is data-driven and, to a certain extent, the character of the residual anomalies reflects the distribution of well control in the vicinity of the fault zones. In cases where dense well control exists near the fault zone, the lateral continuity of the residual anomaly is enhanced. Thus, caution is needed in the interpretation of these results to characterize structural corridors.

In this study, we have used available seismic profiles to validate and characterize the structural corridors. Where potential-field data provides corroborating evidence, this is also considered below.

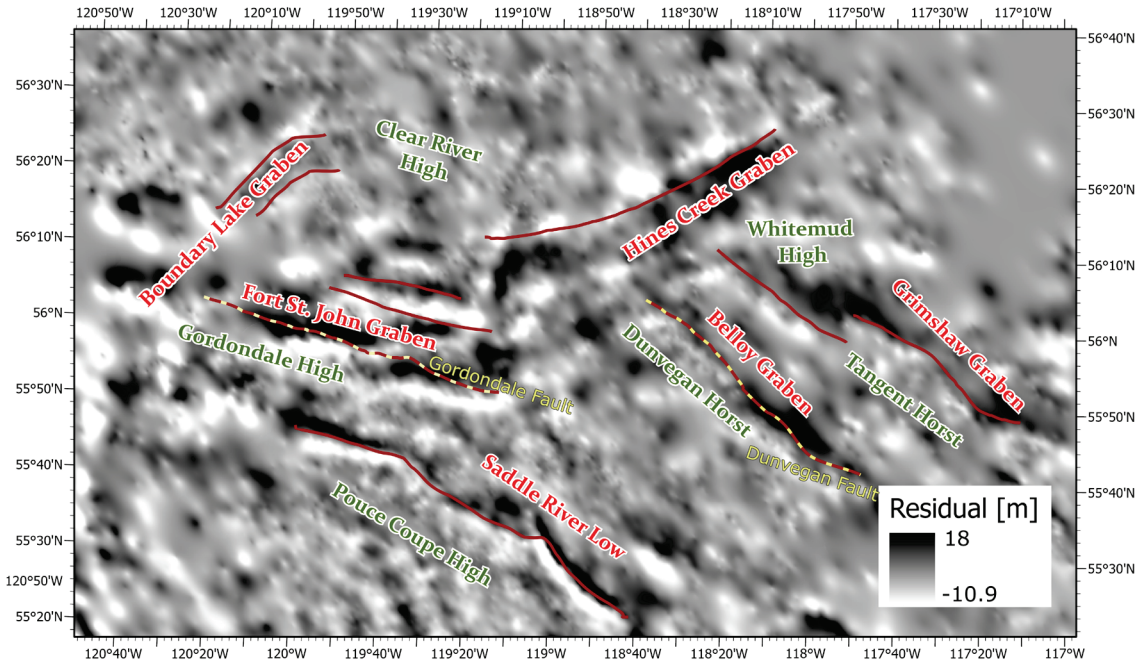

Fig. 10. Enlargement of the Basal Fish Scale Zone residual map in the vicinity of the Dawson Creek Graben Complex (DCGC), showing the primary graben structure (Fort St. John graben, FSJG) and satellite grabens to the north and east. Dip slip fault zones are indicated by a paired positive-negative anomaly, as indicated by the red lines. Gordondale and Dunvegan faults are indicated by the red and yellow lines.

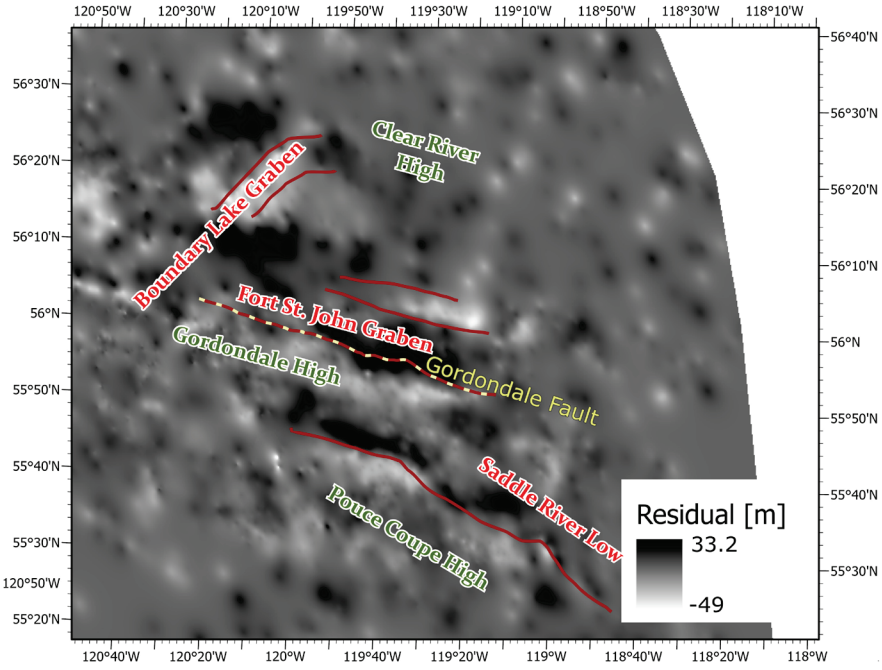

Fig. 11. Enlargement of the Upper Montney residual map in the vicinity of the Dawson Creek Graben Complex (DCGC), showing the primary graben structure (Fort St. John graben, FSJG) and satellite grabens to the north and east. Dip slip fault zones are indicated by a paired positive-negative anomaly, as indicated by the red lines. Gordondale fault is indicated by the red and yellow line.

Seismic Interpretation

Only 2-D seismic profiles are available for this study; hence, it is important to account for the obliquity between the seismic profile and the strike direction of the structural corridor. The available seismic data provide coverage of some parts of the DCGC, but unfortunately no public data are available in other parts of the Montney trend. To view seismic images of the buried thrust belt in the northern Montney play, the reader is referred to Riazi and Eaton (2020). We carry out seismic interpretation starting on the west side of the study area and moving toward the east. The Monias structure has the largest structural relief in the vicinity of the DCGC (Norgard, 1997). Based on published seismic data (Fig. 12), it is characterized by a set of steep, closely spaced, dip-slip faults that terminate upwards into folded Permian and Triassic strata, defining a structural corridor that is estimated to be ~ 6 km in apparent width. Unfortunately, there are no specific details of the seismic line orientation, so it is not possible to calculate the obliquity of the seismic profile with respect to the strike of the feature. The northeast trending Monias structure truncates the roughly east-west trending FSJG, suggesting that the Monias structure is a younger feature. However, fault offsets evident in Fig. 12 suggest initial development of the Monias structure in the late Carboniferous, consistent with other structural elements of the DCGC. More subtle features, characterized by fault hinges in younger sedimentary layers, provide evidence that the Monias structural corridor remained active until the Triassic, and likely until the Late Cretaceous period. In two-way time, the offset of the Debolt and Wabamun horizons in the seismic profile show that these units are displaced by approximately 0.28s TWT. A crude calculation of the corresponding fault offset, assuming an average velocity of 4.5 km/s, yields an estimated net offset of 630m, even though there is no corresponding anomaly in the residual maps (Fig. 8). This illustrates a key limitation of the trend surface residual analysis method, namely that some features are not visible in the residual maps due to limited well control. Finally, in many respects, the Monias structure exemplifies the concept of a structural corridor, as it is clear from seismic data that this is not a single isolated fault, but rather a set of closely spaced, cogenetic faults.

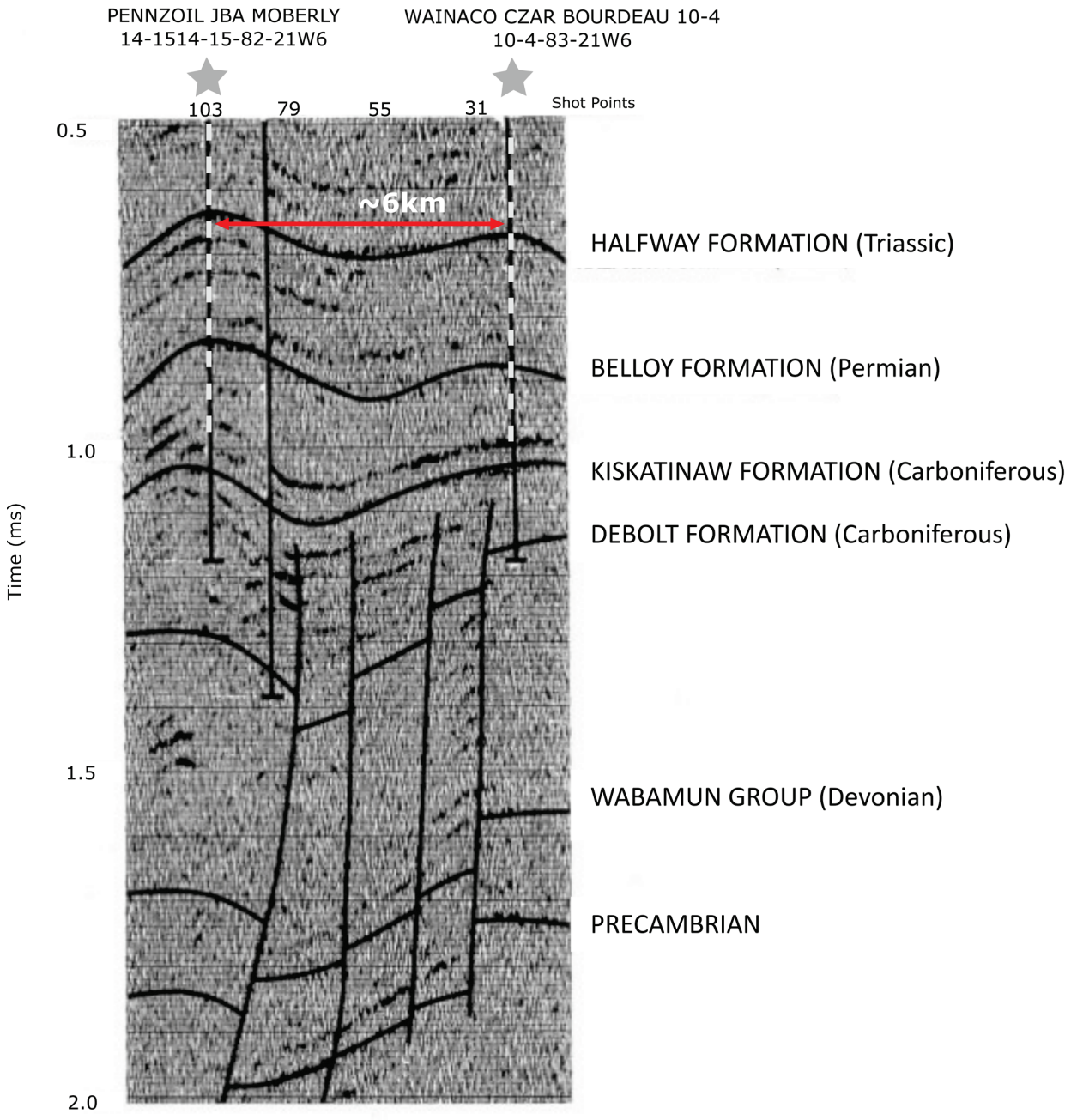

Fig. 12. Seismic section across the Monias structure, forming the northeastern boundary of the Dawson Creek Graben Complex. With a set of closely spaced cogenetic faults and associated fold structures, the Monas structure exemplifies the concept of a structural corridor. Modified from Norgard (1997).

Structural interpretation of the reflection seismic profiles (Fig. 5) included careful analysis of the fault expression on the seismic sections. Specifically, we divided discontinuities on the horizons into 3 classes and marked them on the seismic sections using individual line styles:

- 0th order discontinuity which is the clearest expression of the fault, with easily distinguished throw and hanging wall and footwall (solid line)
- 1st order discontinuity expressed by the fault hinge, which is a more subtle fault signature characterized by continual bend of the horizon (dashed line)
- 2nd order discontinuity defined as the most subtle structural indicator of faulting, represented by the parabolic signature on the seismic section (dotted line)

Figure 13 shows the seismic expression of the southern bounding fault of the FSJG near the Septimus field south of FSJ, BC (profile 'A' in Fig. 5). This profile is nearly perpendicular to the local structural trend of the FSJG and was provided for this study by Pulse Seismic Inc. The structural relief of this corridor is less extreme than the Monias structure, but nevertheless the Debolt horizon (D) exhibits a series of discrete vertical offsets that are interpreted as faults. Using the same method as above, a crude estimate of the net vertical relief is ~ 315m based on ~ 0.14 s offset in two-way time. The interpretation in figure 13 is consistent with previous studies (e.g., Barclay et al., 1990), which show that the southern margin of the FSJG is a series of step-like faults rather than a single fault. The late Carboniferous Stoddart group exhibits thickening within the graben. Shallower faulting, including some antithetic faults, is evident in the seismic data as either truncation of horizontal markers or steep disturbed zones. Taken together, the seismic profile indicates a structural corridor with an apparent width of ~ 8 km.

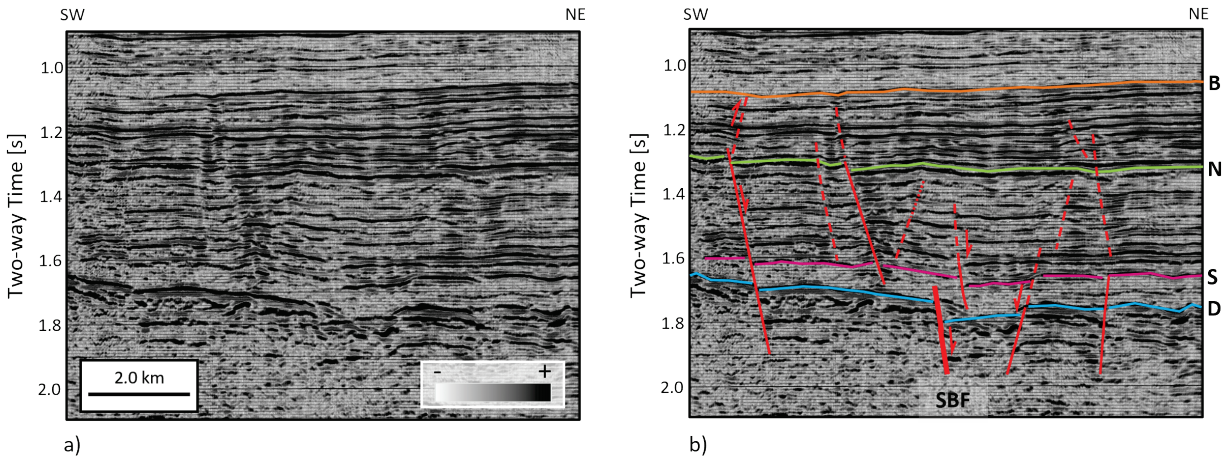

Fig. 13. Seismic profile 'A' across the southern bounding fault (SBF) of the Fort St. John graben (migrated 2-D seismic profile courtesy Pulse Seismic Inc.). Interpreted horizons on the right are Basal Fish Scale Zone (B), the Nordegg Member of Fernie Formation (N), the Stoddart Group (S) and the Debolt Formation (D). Light grey and black colors on the seismic section corresponds to negative and positive relative amplitude, respectively. Apparent width of the structural corridor is approximately 8 km.

Next, we consider a series of profiles from the LITHOPROBE PRAISE transect, starting on the west side and working towards the east. Figure 14 shows line 11A, both uninterpreted and interpreted. The profile shows a series of Devonian horizons, including the Wabamun, that onlap onto the Peace River Arch. Across the arch, there is evidence for numerous faults along the top of Precambrian basement. A number of interpreted faults, the largest being the down-to-the-east Gordondale fault with an estimated slightly less than 200m in vertical throw, define a structural corridor with an apparent width of 53 km. More accurate calculations of apparent vertical throw are given in Appendix A. It is important to realize that the seismic profile is highly oblique to the structural trend, so the actual width of the corridor is much less than the apparent width. Most of the faulting evident in this corridor is located in the upthrown hanging wall of the Gordondale fault, rather than internally within the FSJG.

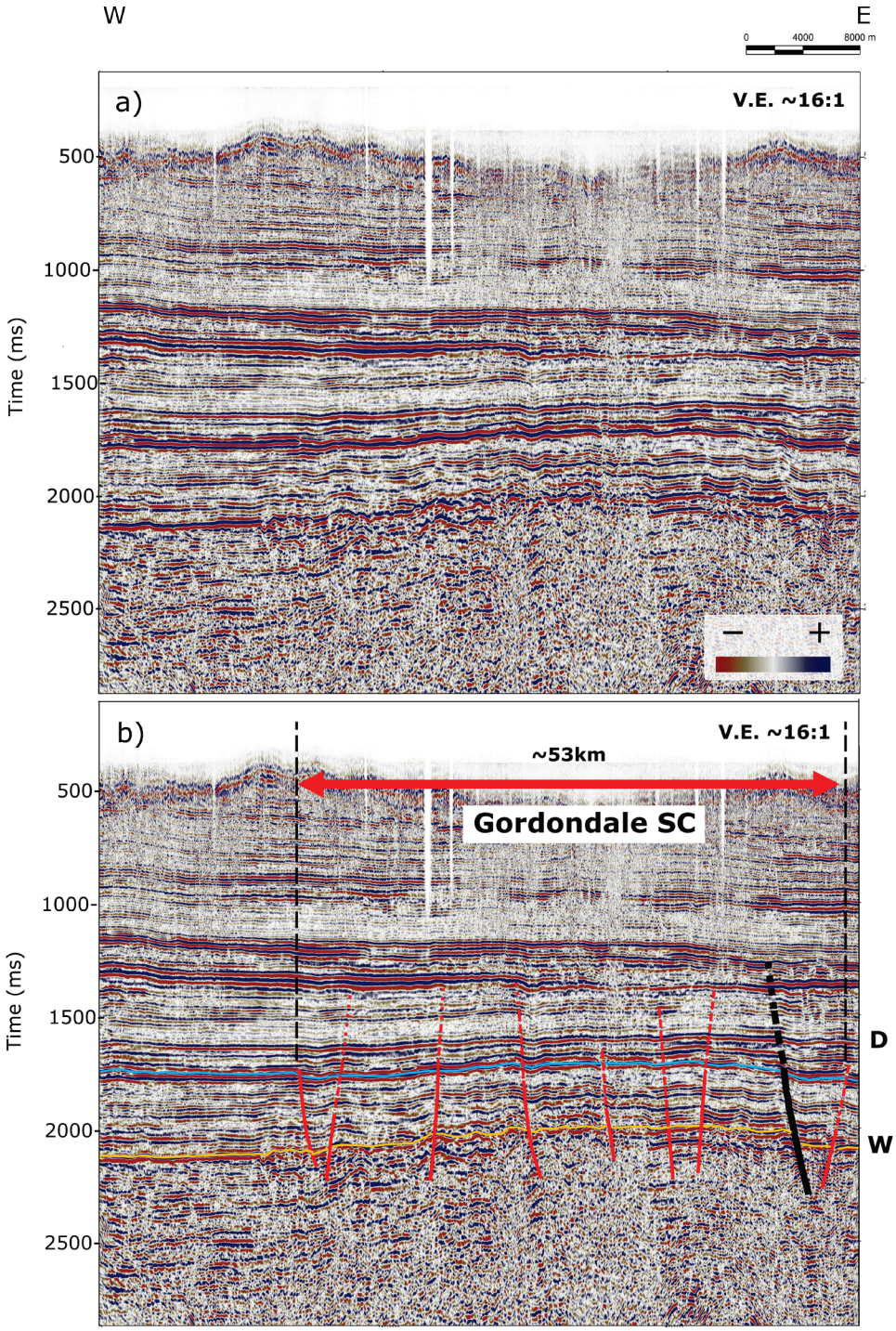

Fig. 14. a) Uninterpreted and b) interpreted seismic profile for LITHOPROBE PRAISE line 11A (migrated). Interpreted horizons on the right are Debolt (D) and Wabamun (W) formations. Red and blue colors on the seismic section corresponds to negative and positive relative amplitude, respectively. Gordondale fault is outlined in black, while secondary faults within Gordondale structural corridor (SC) are marked in red. Apparent width of the Gordondale SC intersecting the profile is approximately 50 km.

Figure 15 shows a second crossing of the Gordondale fault along line 11B, which overlaps slightly with line 11A and is offset a few km to the south (Fig. 5). Based on the offset in the time section, the estimated throw on the Gordondale fault at this point is nearly 270m. To the east, the profile crosses a satellite graben associated with the Rycroft fault (Eaton et al., 1999), which is also crossed on line 12AB (Fig. 16). The vertical throw on the Rycroft fault is considerably less than the Gordondale fault. One potential structural feature which appear on line 12AB is the Berwyn fault located about 16km of the profile. The structure was previously mentioned in the literature (e.g., Mei, 2009), however there are statics artifacts that make the seismic interpretation uncertain.

LITHOPROBE PRAISE line 12CD crosses the entirety of the Dunvegan graben, revealing the lower complexity, asymmetric nature of this satellite graben (Fig. 17). This graben has an approximate maximum down-to-the-east vertical throw of ~ 220m. As with all parts of the DCGC, the graben is filled by sediments of the late Carboniferous Stoddart Group. The eastern margin of the Dunvegan graben is expressed in the seismic profile as breakline defined by a change in dip in the Debolt horizon, rather than a classical fault offset. To the east, there is evidence for additional small-scale faulting in the hanging well. It is notable that the Dunvegan fault correlates spatially with a prominent magnetic anomaly that marks the boundary between the Paleoproterozoic Ksituan and Chinchaga domains (Fig. 4a). Ksituan domain is a clearly defined, structurally deformed positive magmatic arc as opposed to magnetic low within Chinchaga domain (Ekpo et al., 2017, Wright et al, 1994). Although in most cases the top part of the Precambrian basement is poorly imaged due to overprinting by multiple reverberations (Eaton et al., 1995), in this case there appears to be a west-dipping reflection fabric in the upper part of the basement (marked by arrows in Fig. 17). Taken together with evidence from the magnetic map, this suggests that the Dunvegan fault reactivated an older basement structural feature.

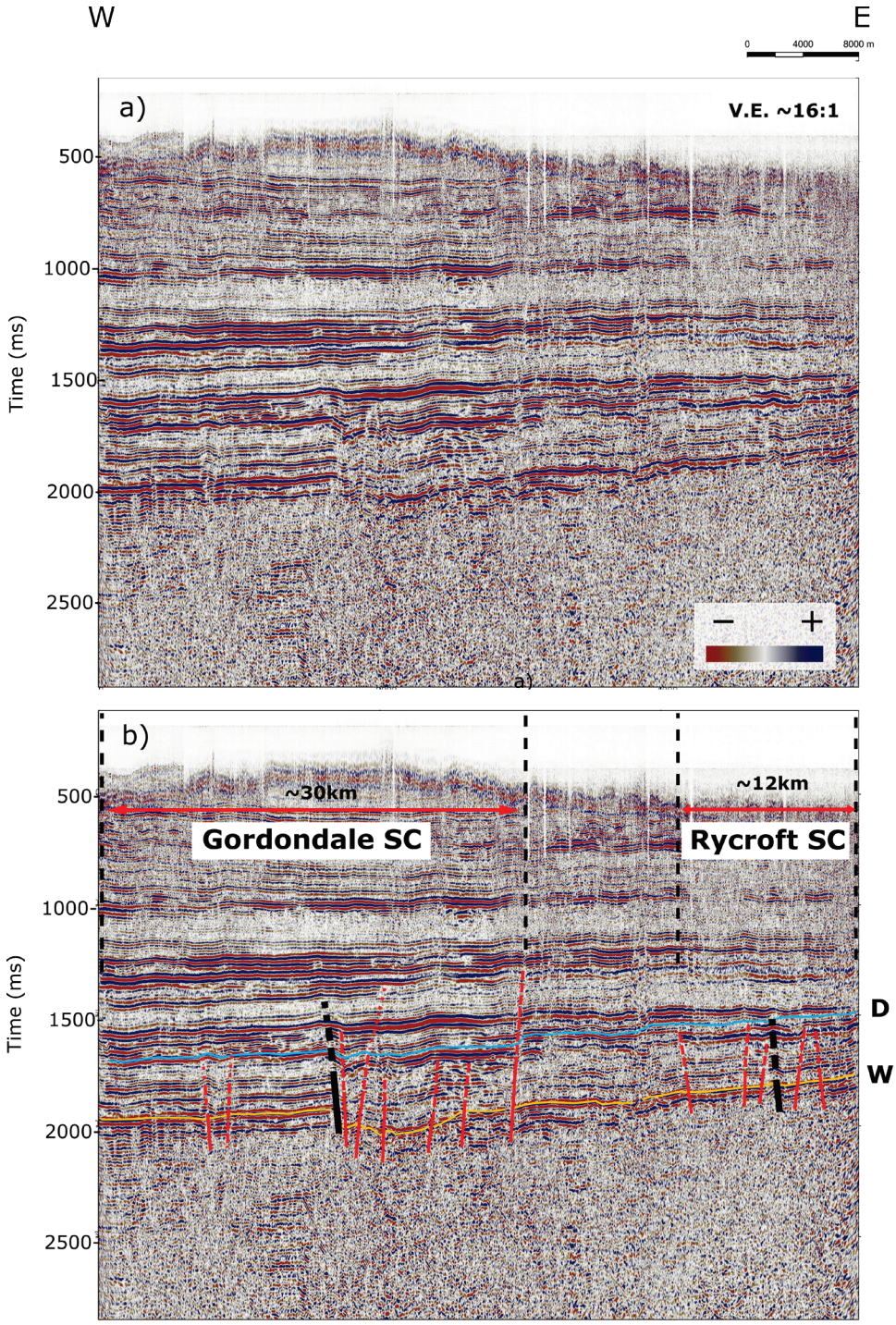

Fig. 15. a) Uninterpreted and b) interpreted seismic profile for LITHOPROBE PRAISE line 11B (migrated). Interpreted horizons on the right are Debolt (D) and Wabamun (W) formations. Red and blue colors on the seismic section corresponds to negative and positive relative amplitude, respectively. Gordondale fault (within Gordondale SC) and Rycroft fault (within Rycroft SC) is outlined in black, while secondary faults within both structural corridors are marked in red. Apparent width of the Gordondale and Rycroft SC intersecting the profile are approximately 30 km and 12 km, respectively).

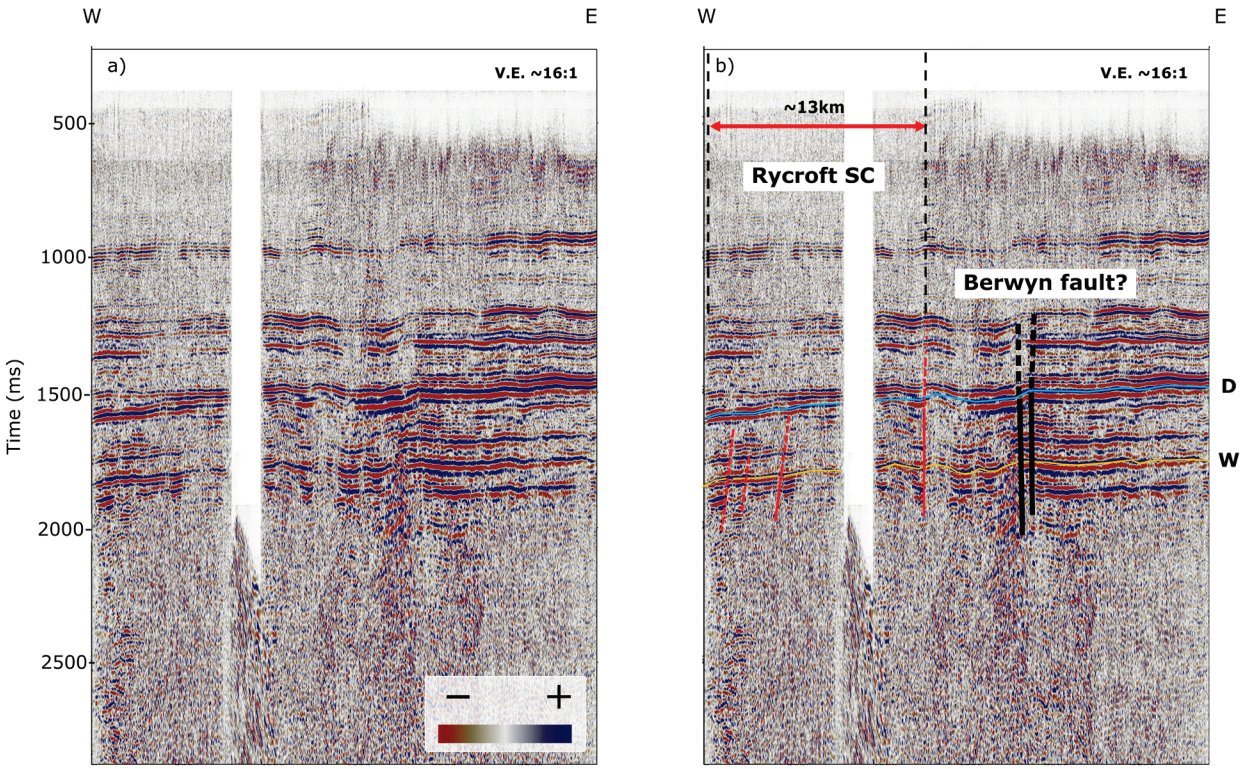

Fig. 16. a) Uninterpreted and b) interpreted seismic profile for LITHOPROBE PRAISE line 12AB (migrated). Interpreted horizons on the right are Debolt (D) and Wabamun (W) formations. Red and blue colors on the seismic section corresponds to negative and positive relative amplitude, respectively. Apparent width of the Rycroft SC intersecting the profile are approximately 13 km. Seismic expression of the structural features potentially associated with primary and secondary Berwyn faults (black line) were identified around 16 km of the profile; however static artifacts make the interpretation less obvious and additional information is required to confirm the presence of the structures.

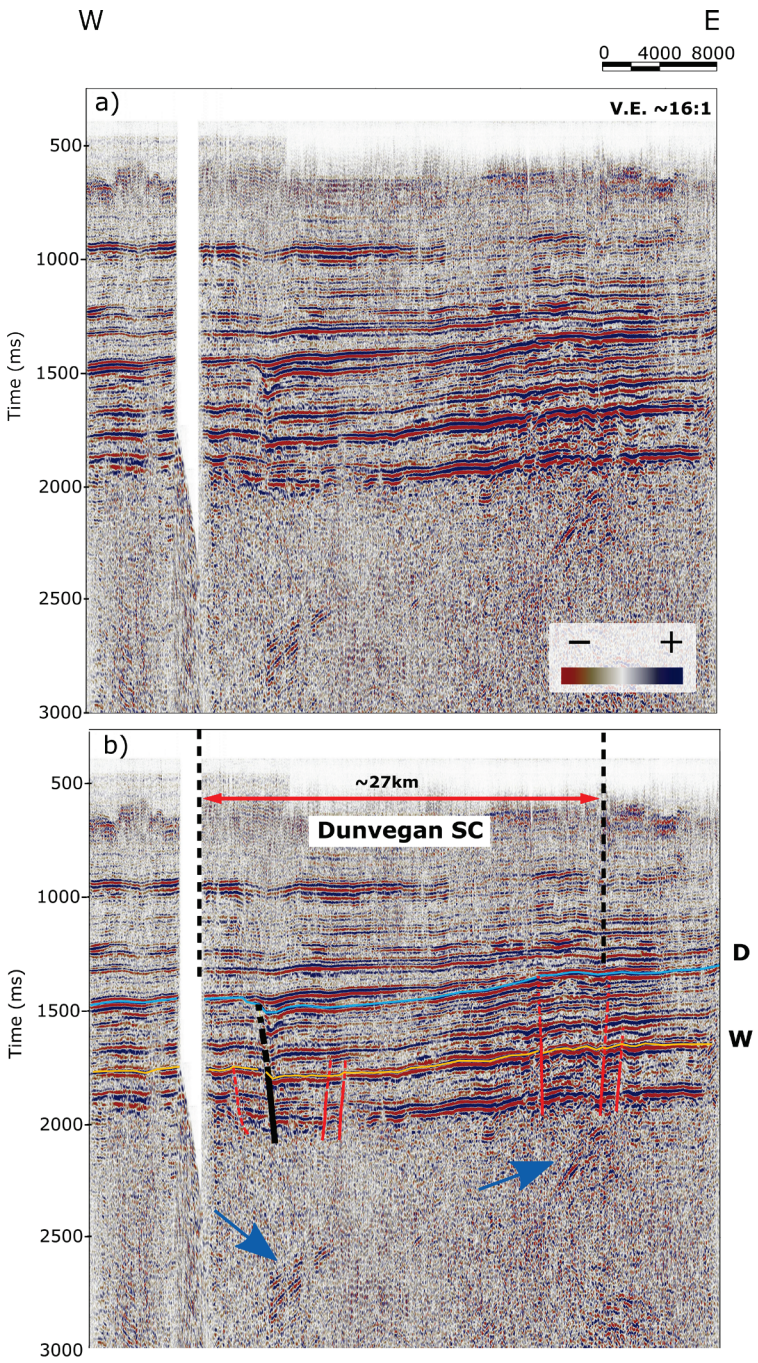

Fig. 17. a) Uninterpreted and b) interpreted seismic profile for LITHOPROBE PRAISE line 12CD (migrated). Interpreted horizons on the right are Debolt (D) and Wabamun (W) formations. Red and blue colors on the seismic section corresponds to negative and positive relative amplitude, respectively. Dunvegan fault is outlined in black, while secondary faults within Dunvegan SC are marked in red. Apparent width of the Dunvegan SC intersecting the profile is approximately 27 km. Blue arrows indicate reflection fabrics associated with Precambrian tectonic deformation of the basement, spatially coincident with a magnetic anomaly trend marking the eastern edge of the Ksituan domain (Fig. 4a).

Figure 18 shows line 12F, which crosses the Tangent fault. This down-to-the-east fault has an apparent vertical throw of more than 300m and marks the edge of another asymmetric satellite graben. The Stoddart Group fill in particularly evident here. As noted by Eaton et al. (1999), the fault appears be marked by a brittle offset of the top of basement, but higher in the section the fault is expressed as a fold. There also appears to be an antithetic fault, as well as a series of smaller structures toward the east that collectively define the Tangent fault corridor. As shown in Fig. 19, the Tangent fault is crossed again in a north-south profile (line 13). Like the east side of the Dunvegan graben, here the fault is expressed as a breakline (change in dip of horizons) rather than a discrete fault offset. This change in the seismic expression of the Tangent fault illustrates the along-strike variation in fault throw that is characteristic of all faults.

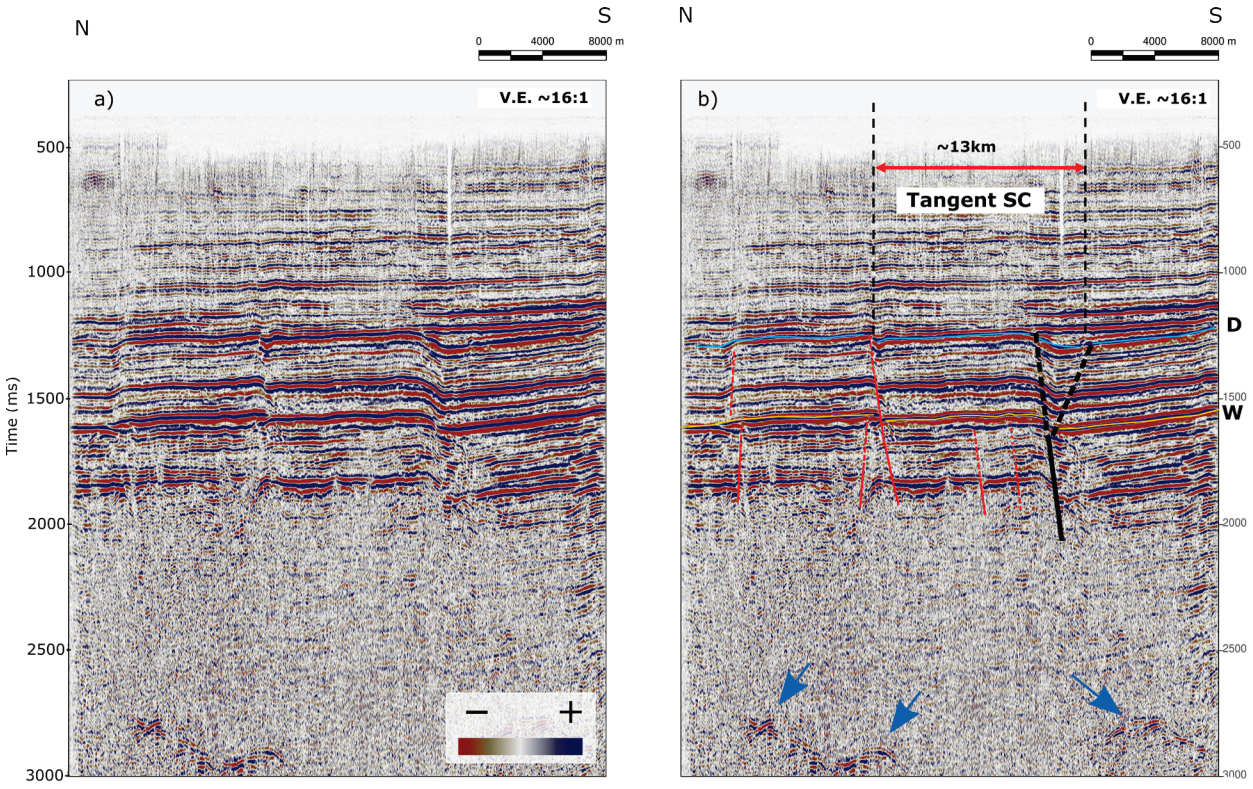

Fig. 18. a) Uninterpreted and b) interpreted seismic profile for LITHOPROBE PRAISE line 12F (migrated). Interpreted horizons on the right are Debolt (D) and Wabamun (W) formations. Red and blue colors on the seismic section corresponds to negative and positive relative amplitude, respectively. Tangent fault is outlined in black, while secondary faults within Tangent SC are marked in red. Apparent width of the Tangent SC intersecting the profile is approximately 13 km. Blue arrows indicate reflection fabrics associated with Precambrian tectonic deformation of the basement, spatially coincident with a magnetic anomaly trend marking the eastern edge of the Ksituan domain (Fig. 4a).

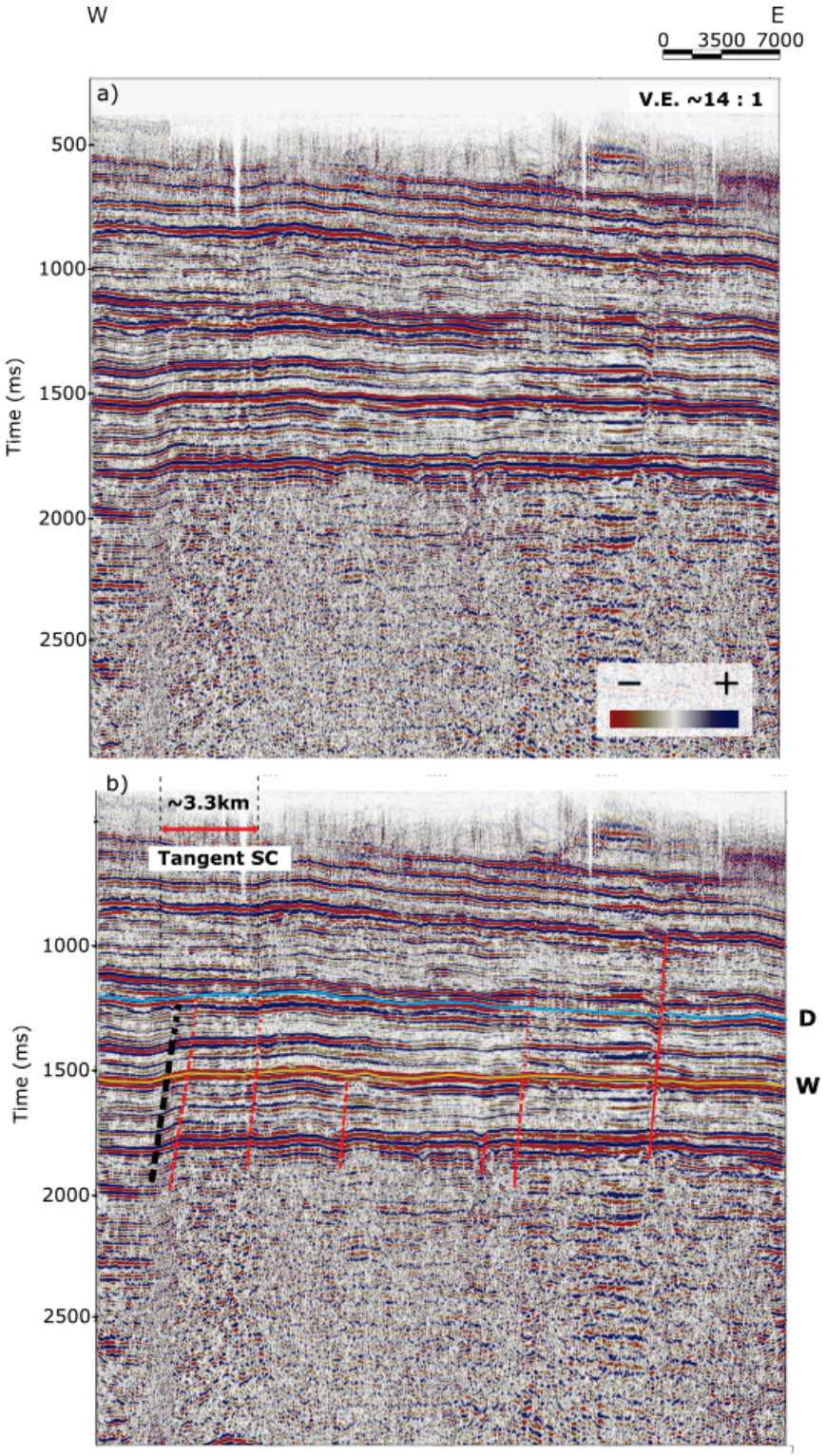

Fig. 19. a) Uninterpreted and b) interpreted seismic profile for LITHOPROBE PRAISE line 13 (migrated). Interpreted horizons on the right are Debolt (D) and Wabamun (W) formations. Red and blue colors on the seismic section corresponds to negative and positive relative amplitude, respectively. Tangent fault is outlined in black, while

secondary faults within Tangent SC are marked in red. Apparent width of the Tangent SC intersecting the profile is approximately 3.3 km.

Discussion

Systematics from seismic data

Seismic interpretation allows the estimation of geometric parameters of structural corridors in the areas intersected by the seismic lines. Widths of the corridors are defined as the apparent values, measured along the profile, while the true values are defined using the angle between directions of the corridor and seismic lines. Table 1 shows length and width of structural corridors, based on seismic interpretation results. Width of the corridors expressed on seismic sections range from ~4km to ~21km and two distinct width groups can be observed. Observed geometrical characteristics were used to investigate potential relationship between length and width of the remaining corridors identified outside of the seismic data. A cross-plot of the length and width are presented in the Figure 20. Based on the limited available data, there is evidence that the width of a structural corridor scales with its length and the positive linear trend is by the relationship: $0.199x - 1.405$, where x corresponds to the length of the corridor in km. Although the limited number of structural corridor examples crossed by seismic profile is not sufficient to confirm the assumed width-length relationship, it is possible to identify increasing trend emerging from the combination of seismic and trend surface analysis results. Corridors intersected by seismic lines can be divided in distinct groups, depending on their widths. Based on general evidence from seismic interpretation, we have implemented a systematic division of the corridors into four distinct groups: 1) Corridors within northern Montney buried thrust and fold zone (TFZ) were assigned widths of 3km; 2) widths of almost all corridors confined within DCGC (except for 3) Gordondale fault, which has width of 12km) were conservatively assigned to be 9km to address the potential location uncertainties and avoid overinterpretation; 4) structural corridors associated with Bovie Lake and Hay River Fault Zone were assigned the width of 24km based on other literature studies of the fault in these regions (e.g. Hayes 2010; Hayes et al., 2021).

It is important to note, that structural studies suggest that segmented fault zones elsewhere are characterized by the scaling relationships between the fault length and vertical displacements (Cowie and Scholtz, 1992; Dawers and Anders, 1995; Kim and Sanderson, 2005), albeit the scaling factors seem to vary within analyzed datasets. Suggested relationships characterizing fault geometries similar to structural corridors could be further used to investigate the relationships displacements of the structures within northeastern BC and Alberta, however it would require additional data including high-density 3D surveys which are currently not publicly available.

Table 1. Geometrical parameters of structural corridors estimated from seismic data. The error margin of 5% reflects the potential incorrect measurements of the length of the corridors from the trend surface analysis or the errors related to the determination of width from the apparent width. To check the details regarding the calculation of the structural corridor width, the reader is referred to *Apparent width calculations* section in Appendix A.

Corridor Name	Length [km]	Width [km]
Gordondale	87.5	14.6 ± 0.7
Rycroft	83.4	15.4 ± 0.8
Dunvegan	94.1	18.2 ± 0.9
Tangent	27.7	4.08 ± 0.2
Monias	36.6	6.4 ± 0.3

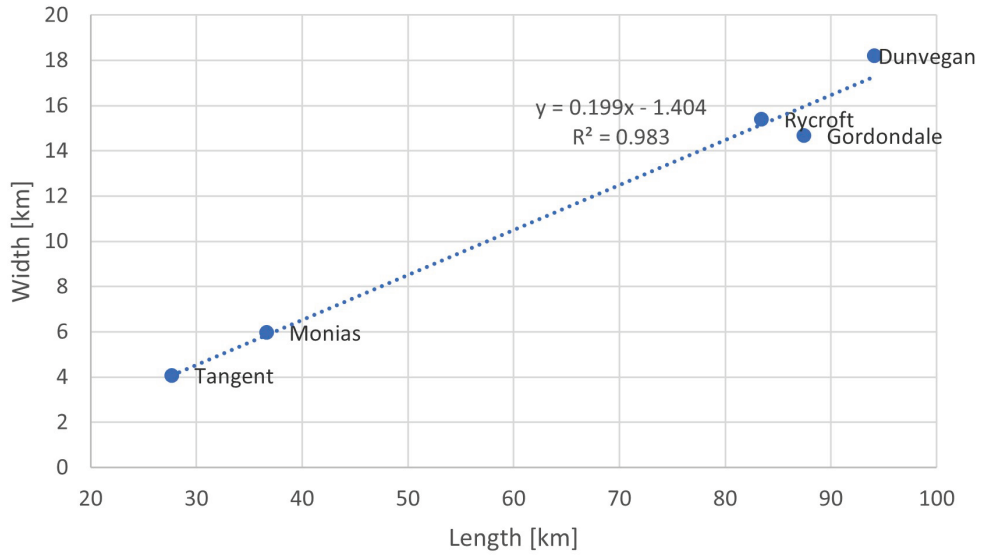

Fig. 20. Relationship between length and half width of the structural corridors. Linear trend is described by the equation $0.199x - 1.404$, where x corresponds to the corridor length.

Structural corridor interpretation

Structural corridors identified using described, multi-step approach overlaid on Debolt and BFSZ residuals are presented in the Figures 21-22. The approach integrates all the available data including trend surface analysis, seismic profiles and published structural corridors based on the literature, addressing the issues spatial limitations of available seismic information within Montney Formation. We have identified three main structural corridor complexes corresponding to the most distinct features in the area: Bovie Fault, Hay River Fault Zone and Dawson Creek Graben Complex. One additional element that was identified on the regional map is the Southern Foreland Thrust Fault Zone, which was most clearly expressed on the Basal Fish Scale Zone residual map (Fig. 22). Although the northern buried lobe of the Foreland Thrust Fault Zone did not show clearly on the residual maps, the presence of the thrust faults in that area (Fig. 1) enables estimation of the extent of the thrust fault zone in that area.

Figure 23 shows an enlargement of structural corridors in the vicinity of the DCGC and the southern Montney, including the main fault zones. The corridors have been numbered and color-coded depending on the source of information. Within DCGC, we have identified 34 main structural corridors and multiple structures within Northern Montney buried TFZ. While the majority of the corridors are characterized by the strong residual contrasts on the residual maps for the Debolt Formation, in the areas outside of DCGC, where the formation top data was insufficient, some structural features were identified on the BFSZ residual map or identified using examples from the literature. The corridors have been numbered and named according to the previous structural interpretations and maps where possible. Remaining corridors were named according to the geographical elements. Details of the interpreted structures are presented in the Table 2.

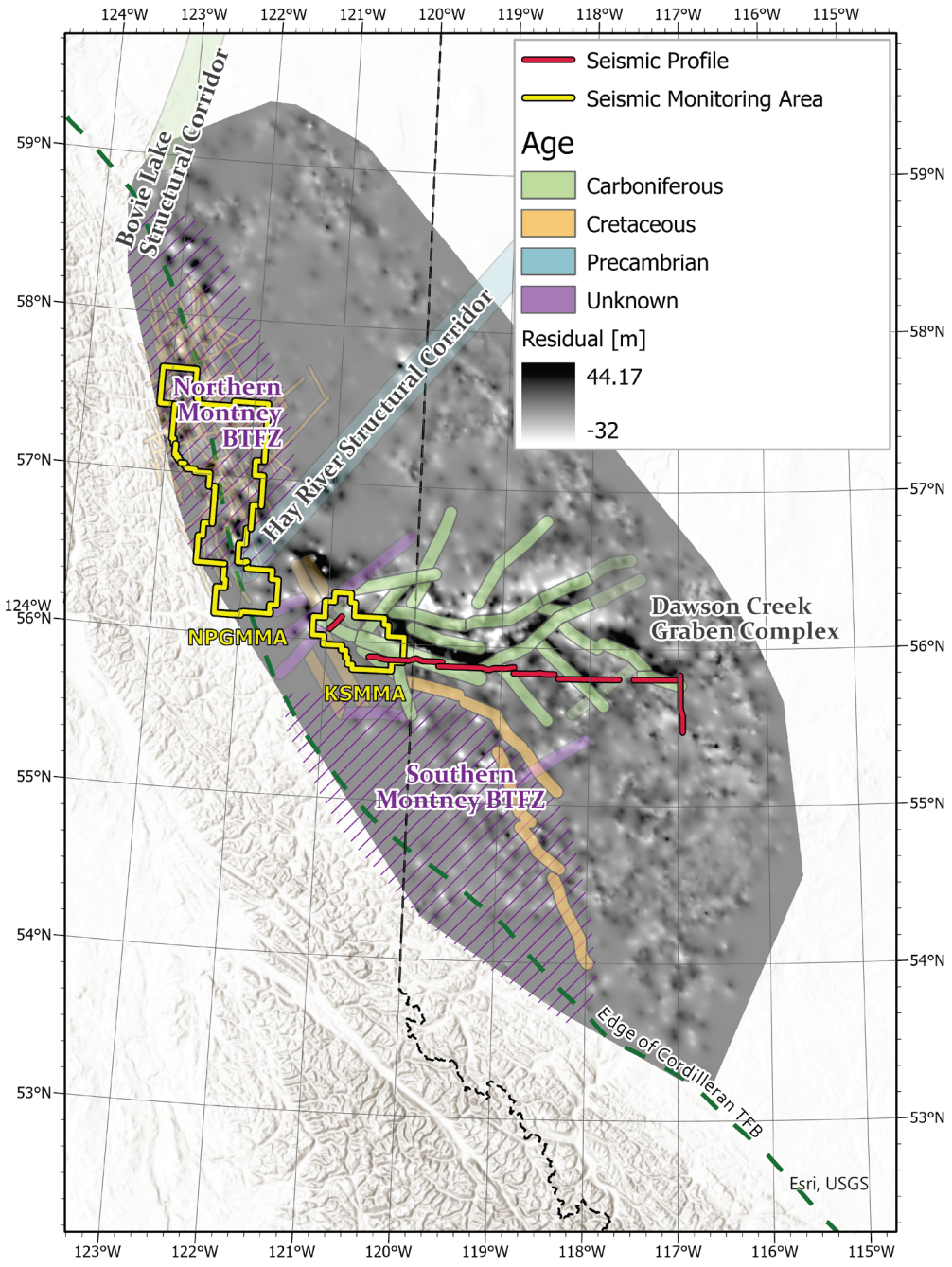

Fig. 21. Regional map of the main structural corridors within study area overlaid on the Debolt residual map. Yellow and red lines indicate the seismic monitoring areas and reflection seismic lines, respectively. The eastern surface limit of the Late Cretaceous – Paleocene Cordilleran thrust and fold belt (TFB) is shown, for reference. Dashed line polygons indicate the extent of the Northern and Southern Montney buried TFB zones. Colors of the structural corridors correspond to the geological age formation when the structural corridor was the formed. Less transparent colors correspond to corridors identified through trend surface analysis, while more transparent features were sourced from previous studies.

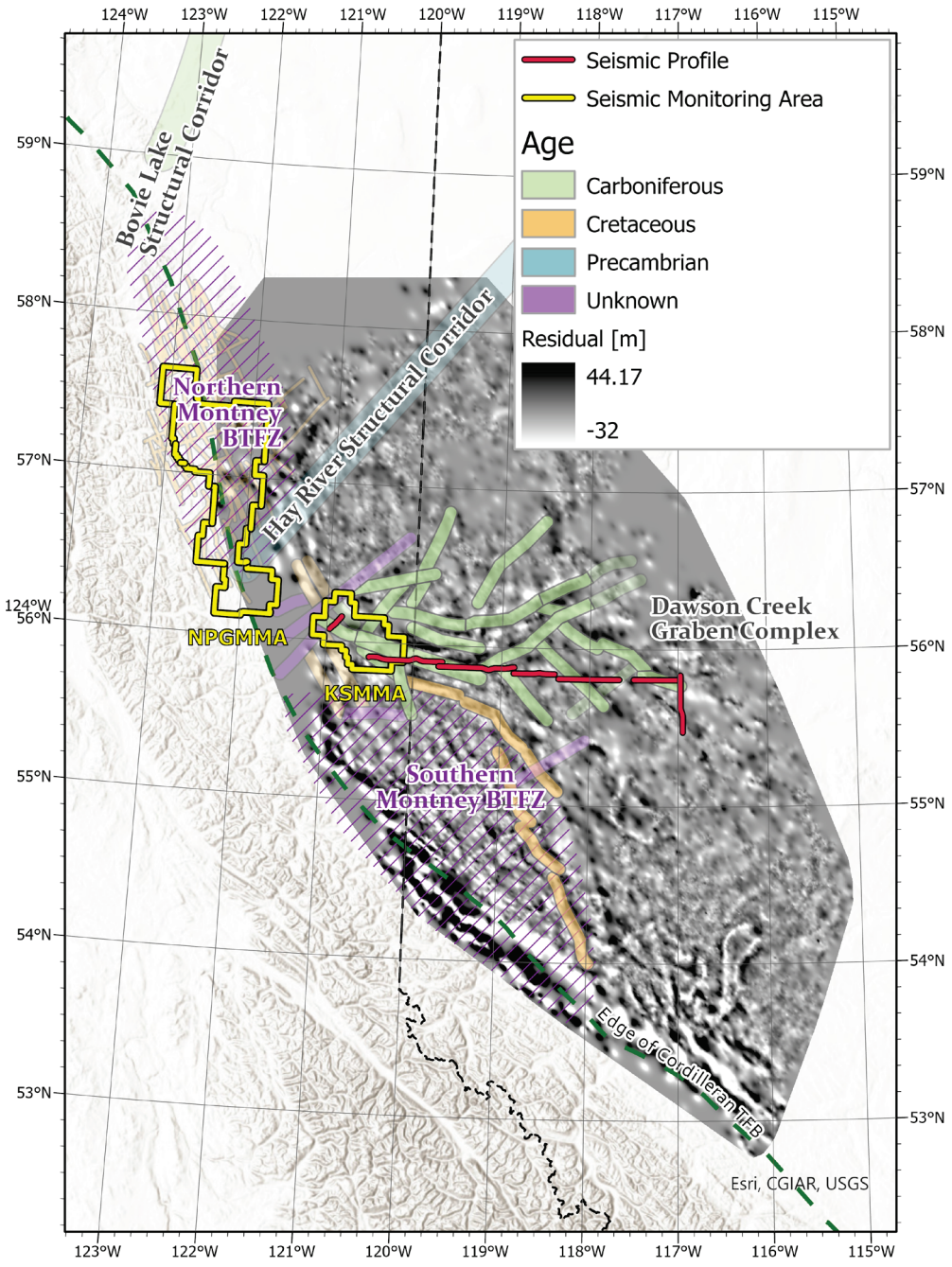

Fig. 22. Regional map of the main structural corridors within study area overlaid on the Basal Fish Scale Zone residual map. Yellow and red lines indicate the seismic monitoring areas and reflection seismic lines, respectively. The eastern surface limit of the Late Cretaceous – Paleocene Cordilleran thrust and fold belt (TFB) is shown, for reference. Dashed line polygons indicate the extent of the Northern and Southern Montney buried TFB zones. Colors of the structural corridors correspond to the geological age when the structural corridor was formed. Less transparent colors correspond to corridors identified through trend surface analysis, while more transparent features were sourced from previous studies. Basal Fish Scale Zone Residual was used to outline structural corridors outside the DCGC, along with the extend of the Southern Montney buried TFZ.

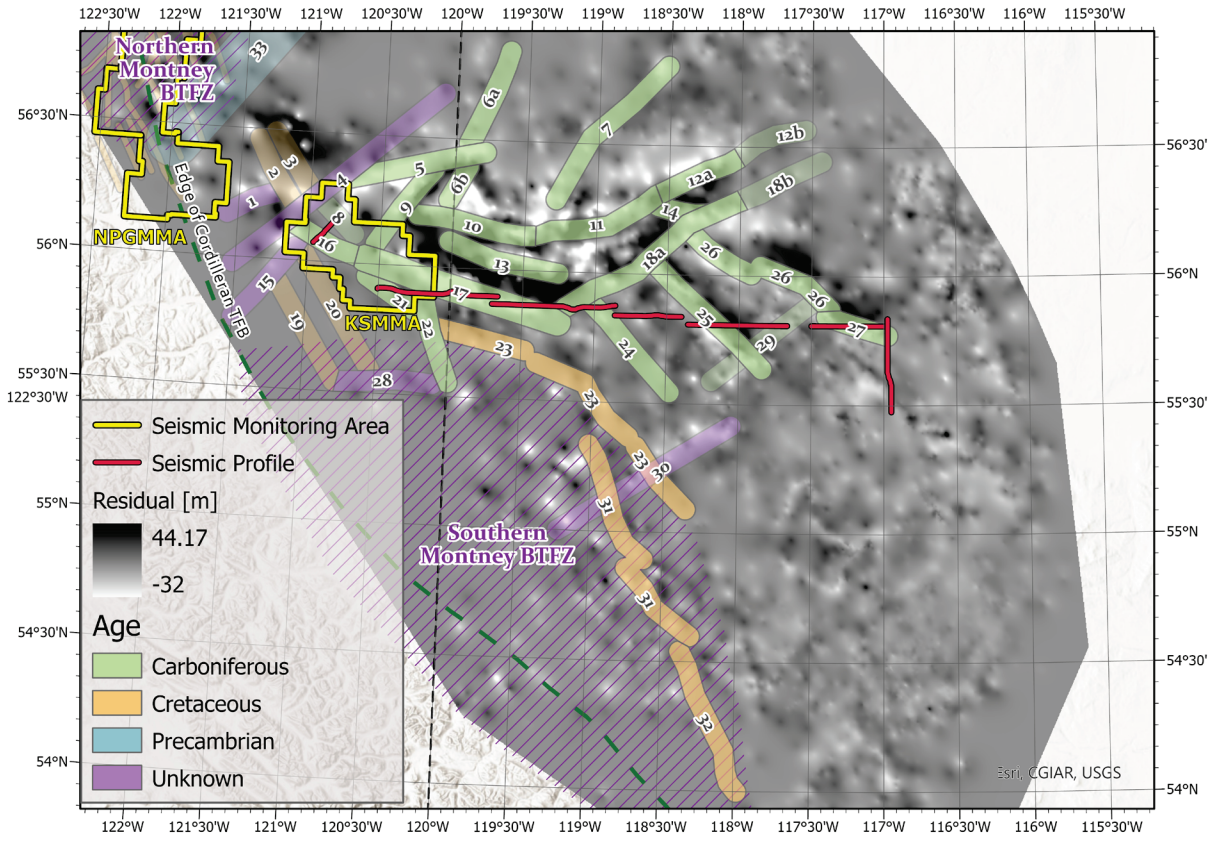

Fig. 23. Map of Debolt Residual within Dawson Creek Graben Complex and southern Montney with overlayed structural corridors and main fault zones. Corridors have been numbered and names are presented in the Table 2. Yellow and red lines indicate the seismic monitoring areas and reflection seismic lines, respectively. The eastern surface limit of the Late Cretaceous – Paleocene Cordilleran TFB is shown, for reference. Dashed line polygons indicate the extent of the Northern and Southern Montney buried TFZ. Colors of the structural corridors correspond to the geological age when the structural corridor was formed. Less transparent colors correspond to corridors identified through trend surface analysis, while more transparent features were sourced from previous studies.

Table 2. The names and horizontal extent assigned to structural corridors is based primarily on past publications and geographical references. Numbers in superscript indicate the original source of the corridor name and/or extent.

Farrell Creek[9]	1	Southern FSJG (a)[8]	18a
North Cache Creek[9]	2	Southern FSJG (b)[10]	18b
Charlie Lake[10]	3	Groundbirch[9]	19
Monias[5]	4	Sunset Creek[9]	20
Pineview[10]	5	Farmington[11]	21
Boundary Lake (a)[8]	6a	Dawson Creek	22
Boundary Lake (b)[10]	6b	Clear River - Pouce Coupe[8]	23
South Whitemud River[9]	7	Rycroft[4]	24
Old Fort[11]	8	Dunvegan[1] / Belloy[2]	25
Flatrock[11]	9	Fairview-Bluesky[8]	26
Bear Canyon[8]	10	Tangent[4]	27
Peace River[10]	11	Brassey Creek[9]	28

Hines Creek (a)[3]	12a	Watino[10]	29
Hines Creek (b)[8]	12b	Grande Prairie[10]	30
Josephine Creek[8]	13	Bear Lake - Smoky River[11]	31
Whitemud[8]	14	Simonette River[11]	32
Pine River[10]	15	HRFZ[9]	33
Septimus[11]	16	Bovie Lake[7]	34
Gordondale[4]	17		

Superscript codes explanations: [1]Lavoie (1958), [2]Sikabonyi and Rodgers (1959), [3]Leckie and Hayes (1990), [4]Richards et al. (1990), [5]Norgard, G. T. (1997), [6]Eaton et al. (1999), [7]MacLean and Morrow (2004), [8]Mei (2009), [9]Davies et al. (2018), [10]Geological Atlas of the Western Canada Sedimentary Basin,[11]Geographic reference (Trend Surface Analysis).

Conclusions

In this study, the regional structural framework of the Montney play (AB and BC) in the WCSB is investigated using an approach that integrates formation tops with geophysical data. The Montney region contains large-scale structural features that are part of the Late Carboniferous Dawson Creek Graben Complex, or the Late Cretaceous – Paleocene Rocky Mountain TFB. Formation tops for seven geological units, from the Late Cretaceous BSFZ to the Late Devonian Wabamun Group, were extracted from the geoSCOUT database. These picks were then carefully screened using a rigorous quality-control process. For each formation top, a residual surface was obtained using trend surface analysis (Mei, 2009) by subtracting a smooth regional trend surface from the QC'd dataset. The regional surface was obtained using ArcGIS based on a 3rd order local polynomial fit to the data. The residual surfaces were then interpolated using kriging analysis. Spatially coherent residual trends were then interpreted to identify regional structures, which are expressed as vertical offsets in the residual surfaces. In areas where seismic data are available, such as LITHOPROBE's PRAISE program, seismic profiles were correlated using well ties and interpreted to characterize and validate the structural elements found from trend surface analysis. This approach shows that structural deformation occurs within corridors that contain systems of co-genetic faults and folds, rather than discrete isolated faults. Magnetic and gravity data show that some, but not all, faults are expressed as potential-field lineaments. Where such correlations are observed, this suggests that the fault corresponds with a tectonic domain boundary in the crystalline basement.

Our analysis yielded 34 major structural corridors that transect the study region and multiple smaller-scale corridors in the Northern part of Montney. Most of these corridors coincide with previously mapped faults, in which case the existing fault name is retained. In some cases, new geographic names are assigned to features that have not previously been recognized in the literature, to our knowledge. The strike-length of each corridor is determined based on the interpretation of trend surface residual maps, while the corridor width is measured from seismic profiles, where available. Where seismic data is not available, corridor

width is estimated using a corridor length-width relationship that we calibrated from the seismic data. To facilitate future comparisons with other datasets, the structural corridors are provided as a GIS shapefile in the digital supplement that accompanies this report (Appendix B). The tectonic history of these structures can be inferred based on the expression of anomalies in each of the trend surface residual maps. For example, structural corridors within the DCGC are expressed most conspicuously in the Debolt residual, but some corridors are expressed more subtly in the BFS residual. This is consistent with seismic evidence for Cretaceous reactivation of Late Carboniferous normal faults.

In addition to the aforementioned structural corridors, we also observed an orogen-parallel structural fabric within the BFS residual map, in the foreland of the Rocky Mountain TFB and south of the DCGC. Although no internal structural corridors are interpreted within this lobate region, the eastern margin of this zone is delineated by several distinct structural corridors. This lobate region is interpreted as a buried foreland TFB, possibly associated with intercutaneous wedging (Skuce, 1996). A similar buried thrust belt has been identified north of the DCGC (Riazi and Eaton, 2020), as shown in Fig. 1. The weak (or absent) expression of this region at deeper stratigraphic levels indicates that either faults sole out above the deeper formation investigated here, or there is insufficient well control to resolve this structural fabric at deeper stratigraphic horizons. Nevertheless, the documentation in this study of a buried frontal foothills structural zone to the south of the DCGC, evidently similar to a known buried structural zone in the northern Montney, provides an indication of the utility of this type of analysis.

There are several important assumptions and limitations of our analysis that must be considered. Both the trend surface residual method (using formation tops) and interpretation of seismic profiles are best suited to characterize faults with vertical offset. Thus, it is likely that strike-slip structures have been missed. In addition, trend surface residual analysis and seismic interpretation suffer from other resolution constraints. The trend surface analysis is limited by the spatial resolution afforded by well control; for example, it is clear that the Basal Fish Scale Zone residual map has both better spatial resolution and more uniform coverage than the deeper horizons. Similarly, seismic interpretations are constrained by both the limited availability of seismic data as well as its inherent low vertical resolution limit (minimum resolvable fault offset of approximately 40m, in the case of the LITHOPROBE profiles considered here). This implies that many ‘subseismic’ faults may exist that could be incorporated in the analysis within the context of fault scaling relationships and structural corridors (e.g., Gauthier and Lake, 1993). Ultimately, our analysis provides a structural model that can be further examined and tested with new data as it becomes available.

Acknowledgements

The authors would like to thank Pulse Seismic Inc. for allowing the publication of seismic profile A in this report. Mark Cooper, Mark Hayes and Taylor Mennis are thanked for valuable discussions regarding formation tops catalogues. Authors would like to also thank Michelle Gaucher and Stu Venables for their valuable insigths. Authors would like to also acknowledge the Natural Resources Canada Geoscience for New Energy Supply (GNES) program and Geoscience BC for providing the financial support for this research. geoLOGIC Systems is sincerely thanked for providing access to the geoSCOUT database used in this work.

References

Ackermann, R. V., Schlische, R. W., & Withjack, M. O. (2001). The geometric and statistical evolution of normal fault systems: an experimental study of the effects of mechanical layer thickness on scaling laws. *Journal of Structural Geology*, 23(11), 1803-1819.

Allen, D., Bustin, A. & Eberhart, E. (2019). Scientific Review of Hydraulic Fracturing in British Columbia. https://www2.gov.bc.ca/assets/gov/farming-natural-resources-and-industry/natural-gas-oil/responsible-oil-gas-development/scientific_hydraulic_fracturing_review_panel_final_report.pdf Accessed 2021/07/16.

Atkinson, G. M., Eaton, D. W., Ghofrani, H., Walker, D., Cheadle, B., Schultz, R., Shcherbakov, R., Tiampo, K., Gu, J., Harrington, R., Liu, Y., van der Baan, M. & Kao, H. (2016). Hydraulic fracturing and seismicity in the Western Canada Sedimentary Basin. *Seismological Research Letters*, 87(3), 631-647.

Bao, X., & Eaton, D. W. (2015). Large variations in lithospheric thickness of western Laurentia: Tectonic inheritance or collisional reworking?. Precambrian Research, 266, 579-586.

Bao, X., Eaton, D. W., & Guest, B. (2014). Plateau uplift in western Canada caused by lithospheric delamination along a craton edge. *Nature Geoscience*, 7(11), 830-833.

Beranek, L.P., Mortensen, J.K., Orchard, M.J. & Ullrich, T. (2010). Provenance of North American Triassic strata from west-central and southeastern Yukon: correlations with coeval strata in the Western Canada Sedimentary Basin and Canadian Arctic Islands. Canadian Journal of Earth Sciences, 47, 53–73.

Barclay, J. E., Krause, F. F., Campbell, R. I., & Utting, J. (1990). Dynamic casting of a graben complex: basin infill and differential subsidence during the Permo–Carboniferous, Peace River Embayment, western Canada. *Bulletin of Canadian Petroleum Geology*, 38, 115-145.

BC OGC. (2014). Investigation of observed seismicity in the Montney Trend. BC Oil and Gas Commission.

Bense, V. F., Gleeson, T., Loveless, S. E., Bour, O., & Scibek, J. (2013). Fault zone hydrogeology. *Earth-Science Reviews*, 127, 171-192.

Butler, R. W. (1985). The restoration of thrust systems and displacement continuity around the Mont Blanc Massif, NW external Alpine thrust belt. *Journal of Structural Geology*, 7(5), 569-582.

Chang, K. W., & Segall, P. (2016). Seismicity on basement faults induced by simultaneous fluid injection–extraction. *Pure and Applied Geophysics*, 173(8), 2621-2636.

Cowie, P. A., & Scholz, C. H. (1992). Displacement-length scaling relationship for faults: data synthesis and discussion. *Journal of Structural Geology*, 14(10), 1149-1156.

Crombez, V., Rohais, S., Baudin, F. & Euzen, T. (2016). Facies, welllog patterns, geometries and sequence stratigraphy of a wave-dominated margin: insight from the Montney Formation (Alberta, British Columbia, Canada). Bulletin of Canadian Petroleum Geology, 64, 516–537.

Davies, G.R. (1997). The Triassic of the Western Canadian Sedimentary Basin: Tectonic and stratigraphic framework, palaeogeography, palaeoclimate and biota. Bulletin of Canadian Petroleum Geology, 45, 434–460.

Davies, G.R., Moslow, T.F. & Sherwin, M.D. (1997). The Lower Triassic Montney Formation, west central Alberta. Bulletin of Canadian Petroleum Geology, 45, 474–505.

Davies, G. R., & Smith, L. B. (2006). Structurally controlled hydrothermal dolomite reservoir facies: An overview. AAPG bulletin, 90(11), 1641-1690.

Davies, G.R., Watson, N., Moslow, T.F. & MacEachern, J.A. (2018). Regional subdivisions, sequences, correlations and facies relationships of the Lower Triassic Montney Formation, west-central Alberta to northeastern British Columbia, Canada – with emphasis on role of palaeostructure. Bulletin of Canadian Petroleum Geology, 66, 23–92.

Dawers, N. H., & Anders, M. H. (1995). Displacement-length scaling and fault linkage. *Journal of Structural Geology*, 17(5), 607-614.

Dix, G. R. (1993). Patterns of burial-and tectonically controlled dolomitization in an Upper Devonian fringing-reef complex; Leduc Formation, Peace River Arch area, Alberta, Canada. *Journal of Sedimentary Research*, 63(4), 628-640.

Drivet, E., & Mountjoy, E. W. (1997). Dolomitization of the Leduc Formation (Upper Devonian), southern Rimbey-Meadowbrook reef trend, Alberta. *Journal of Sedimentary Research*, 67(3), 411-423.

Ducros, M., Sassi, W., Vially, R., Euzen, T., Crombez, V., 2017. 2-D basin modeling of the Western Canada sedimentary basin across the Montney-Doig system: Implications for hydrocarbon migration pathways and unconventional resources potential, in: AbuAli, M.A., Moretti, I., Nordgård Bolås, H.M. (Eds.), Petroleum Systems Analysis—Case Studies: AAPG Memoir 114. The American Association of Petroleum Geologists, pp. 117–134. https://doi.org/10.1306/13602027M1143703.

Duggan, J. P., Mountjoy, E. W., & Stasiuk, L. D. (2001). Fault-controlled dolomitization at Swan Hills Simonette oil field (Devonian), deep basin west-central Alberta, Canada. *Sedimentology*, 48(2), 301-323.

Eaton, D. W., Milkereit, B., Ross, G. M., Kanasewich, E. R., Geis, W., Edwards, D. J., ... & Varsek, J. (1995). Lithoprobe basin-scale seismic profiling in central Alberta: Influence of basement on the sedimentary cover. *Bulletin of Canadian Petroleum Geology*, *43*(1), 65-77.

Eaton, D.W. (2018). *Passive seismic monitoring of induced seismicity: Fundamental principles and application to energy technologies*. Cambridge University Press.

Eaton, D. W., Ross, G. M., & Hope, J. (1999). The rise and fall of a cratonic arch: A regional seismic perspective on the Peace River Arch, Alberta. Bulletin of canadian petroleum geology, 47(4), 346-361.

Eaton, D. W., & Schultz, R. (2018). Increased likelihood of induced seismicity in highly overpressured shale formations. *Geophysical Journal International*, 214(1), 751-757.

Edwards, D.E., Barclay, J.E., Gibson, D.W., Kvill, G.E. & Halton, E. (1994). Triassic strata of the Western Canadian Sedimentary Basin. In: Mossop, G. & Shetsen, I. (Eds.) Geological atlas of the Western Canada Sedimentary Basin (I). Canadian Society of Petroleum Geologists and Alberta Research Council, Special Report 4, pp. 159–275.

Edwards, D. J., Lyatsky, H. V., & Brown, R. J. (1998). Regional interpretation of steep faults in the Alberta Basin from public-domain gravity and magnetic data: an update. Canadian Society of Exploration Geophysicists, 23(1), 15-24.

Ekpo, E., Eaton, D., & Weir, R. (2017). Basement tectonics and fault reactivation in Alberta based on seismic and potential field data. In: *Geophysics*, Okiwelu, A. (ed.), InTech Open. DOI: 10.5772/intechopen.72766.

Fan, Z., Eichhubl, P., & Gale, J. F. (2016). Geomechanical analysis of fluid injection and seismic fault slip for the Mw4. 8 Timpson, Texas, earthquake sequence. *Journal of Geophysical Research: Solid Earth*, 121(4), 2798-2812.

Ferri, F. & Zonneveld, J.-P. (2008). Were Triassic rocks of the Western Canada Sedimentary Basin deposited in a foreland? Canadian Society of Petroleum Geologists Reservoir, 35, 12–14.

Fox, A. D. & Watson, N. D. (2019). Induced Seismicity Study in the Kiskatinaw Seismic Monitoring and Mitigation Area, British Columbia.

Gale, J. F., Laubach, S. E., Olson, J. E., Eichhubl, P., & Fall, A. (2014). Natural fractures in shale: A review and new observations. *AAPG Bulletin*, 98(11), 2165–2216. https://doi.org/10.1306/08121413151

Gauthier, B. D. M., & Lake, S. D. (1993). Probabilistic modeling of faults below the limit of seismic resolution in Pelican Field, North Sea, offshore United Kingdom. *AAPG Bulletin*, 77(5), 761-777.

Gibson, D.W. & Barclay, J.E. (1989). Middle Absaroka Sequence – the Triassic stable craton. In: Ricketts, B.D. (Ed.) Western Canada Sedimentary Basin – A Case History, Canadian Society of Petroleum Geologists, Special Publication, 30, 219–232.

Golding, M.L., Mortensen, F., Ferri, F., Zonneveld, J.-P. & Orchard, M.J. (2016). Determining the provenance of Triassic sedimentary rocks in northeastern British Columbia and western Alberta using detrital zircon geochronology, with implications for regional tectonics. Canadian Journal of Earth Science, 53, 140–155.

Goodacre, A. K., Grieve, R. A., Halpenny, J. F., & Warren, L. A. (1987). Isostatic gravity anomaly map of Canada. NRCan Surveys and Mapping Branch.

Green, D. G., & Mountjoy, E. W. (2005). Fault and conduit controlled burial dolomitization of the Devonian west-central Alberta Deep Basin. *Bulletin of Canadian Petroleum Geology*, 53(2), 101-129.

Hansom, J., & Lee, M. K. (2005). Effects of hydrocarbon generation, basal heat flow and sediment compaction on overpressure development: a numerical study. Petroleum Geoscience, 11(4), 353-360.

Hart, B. S., Marfurt, K. J., Varban, B. L., & Plint, A. G. (2007). Blind thrusts and fault-related folds in the Upper Cretaceous Alberta Group, deep basin, west-central Alberta: implications for fractured reservoirs. *Bulletin of Canadian Petroleum Geology*, 55(2), 125-137.

Hayba, D. O., Bethke, P. M., Heald, P., & Foley, N. K. (1985). The geological, mineralogical and geochemical characteristics of volcanic-hosted epithermal deposits: *Reviews in Economic Geology*, v. 2.

Hayes, B.J. (2010): Horn River Basin aquifer characterization project, northeastern British Columbia (NTS 094I, J, O, P): progress report; in Geoscience BC Summary of Activities 2009, Geoscience BC, Report 2010-1, p. 245–248.

Hayes, B.J., Macleod S. and Carey J. Characterization of Belloy, Kiskatinaw and Debolt water disposal zones in the Montney play area, northeastern British Columbia; in Geoscience BC Summary of Activities 2014, Geoscience BC, Report 2015-1, p. 85–88, 2015.

Hayes, B.J., Anderson, J.H., Cooper, M., McLellan, P.J., Rostron, B. and Clarke, J. (2021): Wastewater disposal in the maturing Montney play fairway, northeastern British Columbia (NTS 093P, 094A, B, G, H); in Geoscience BC Summary of Activities 2020: Energy and Water, Geoscience BC, Report 2021-02, p. 91–102.

Henderson, C.M., Golding, M.L. & Orchard, M.J. (2018). Conodont sequence biostratigraphy of the Lower Triassic Montney Formation. Bulletin of Canadian Petroleum Geology, 66, 7–22.

Hennings, P. H., Lund Snee, J. E., Osmond, J. L., DeShon, H. R., Dommisse, R., Horne, E., Lemons, C. & Zoback, M. D. (2019). Injection-induced seismicity and fault-slip potential in the Fort Worth Basin, Texas. *Bulletin of the Seismological Society of America*, 109(5), 1615-1634.

Hope, J., Eaton, D. W., & Ross, G. M. (1999). Lithoprobe seismic transect of the Alberta Basin: Compilation and overview. *Bulletin of Canadian Petroleum Geology*, 47(4), 331-345.

Hope, J., & Eaton, D. (2002). Crustal structure beneath the Western Canada Sedimentary Basin: constraints from gravity and magnetic modelling. *Canadian Journal of Earth Sciences*, 39(3), 291-312.

Hyndman, R. D., & Currie, C. A. (2011). Why is the North America Cordillera high? Hot backarcs, thermal isostasy, and mountain belts. *Geology*, 39(8), 783-786.

Kanamori, H., & Anderson, D. L. (1975). Theoretical basis of some empirical relations in seismology. *Bulletin of the Seismological Society of America*, 65(5), 1073-1095.

Kim, Y. S., & Sanderson, D. J. (2005). The relationship between displacement and length of faults: a review. Earth-Science Reviews, 68(3-4), 317-334.

Lavoie, D. H. (1958). The Peace River Arch during Mississippian and Permo-Pennsylvanian time. Alberta Society of Petroleum Geologists. Journal, 6, 211-251.

Law, B. E., & Dicknson, W. W. (1985). Conceptual model for origin of abnormally pressured gas accumulations in low-permeability reservoirs. AAPG bulletin, 69(8), 1295-1304.

Le Guerroué, E., & Cobbold, P. R. (2006). Influence of erosion and sedimentation on strike-slip fault systems: insights from analogue models. *Journal of Structural Geology*, 28(3), 421-430.

Liseroudi, M. H., Ardakani, O. H., Sanei, H., Pedersen, P. K., Stern, R. A., & Wood, J. M. (2020). Origin of sulfate-rich fluids in the Early Triassic Montney Formation, Western Canadian Sedimentary Basin. *Marine and Petroleum Geology*, 114, 104236.

Lyatsky, H. V., Pană, D. I., & Grobe, M. (2005). Basement structure in central and southern Alberta: Insights from gravity and magnetic maps. Alberta Energy and Utilities Board.

MacLean, B. C., & Morrow, D. W. (2004). Bovie Structure: its evolution and regional context. Bulletin of Canadian Petroleum Geology, 52(4), 302-324.

Mei, S. (2009). New insights on faults in the Peace River Arch region, northwest Alberta, based on existing well-log data and refined trend surface analysis. *Canadian Journal of Earth Sciences*, 46(1), 41-65.

Miall, A.D. & Blakey, R.C. (2008), The Phanerozoic tectonic and sedimentary evolution of North America. In: Miall, A.D. (Ed.) Sedimentary Basins of United States and Canada. Amsterdam: Elsevier, pp. 1–29.

Morley, C. K. (2002). Evolution of large normal faults: Evidence from seismic reflection data. *AAPG Bulletin*, 86(6), 961-978.

Morris, N., Asgar-Deen, M., Gardner, D. & Glemser, C. (2018). A preliminary investigation of the igneous origins of the Montney and Doig formations: Integrating igneous geochemistry techniques for interpreting sedimentary provenance. Bulletin of Canadian Petroleum Geology, 66, 161–174.

Moslow, T.F. & Davies, G.R. (1997). Turbidite reservoir facies in the Lower Montney Formation, west-central Alberta. In: Moslow, T.F. & Wittenberg, J. (Eds.) Triassic of the Western Canada Sedimentary Basin, Bulletin of Canadian Petroleum Geology, 45, 507–536.

Moslow, T.F., Haverslew, B. and Henderson, C.M. (2018). Sedimentary facies, petrology, reservoir characteristics, conodont biostratigraphy and sequence stratigraphic framework of a continuous (395,) full diameter core of the Lower Triassic Montney Fm, northeastern British Columbia. Bulletin of Canadian Petroleum Geology, 66, 259–287.

National Energy Board. (2013). Energy briefing note: The ultimate potential for unconventional petroleum from the Montney Formation of British Columbia and Alberta.

Norgard, G. T. (1997). Structural inversion of the Middle Triassic Halfway Formation, Monias Field, northeast British Columbia. *Bulletin of Canadian Petroleum Geology*, 45(4), 614-623.

O'Connell, S. C. (1990). The development of the Lower Carboniferous Peace River Embayment as determined from Banff and Pekisko formation depositional patterns. *Bulletin of Canadian Petroleum Geology*, 38(1), 93-114.

O'Connor, M. J., & Gretener, P. E. (1974). Differential compaction within the Woodbend Group of central Alberta. Bulletin of Canadian Petroleum Geology, 22(3), 269-304.

Onajite, E. (2013). Seismic data analysis techniques in hydrocarbon exploration. Elsevier.

Pană, D. I. (2003). Precambrian Basement of the Western Canada Sedimentary Basin in Northern Alberta.

Pană, D. I., & van der Pluijm, B. A. (2015). Orogenic pulses in the Alberta Rocky Mountains: Radiometric dating of major faults and comparison with the regional tectono-stratigraphic record. *GSA Bulletin*, 127(3-4), 480-502.

Pilkington, M., Miles, W. F., Ross, G. M., & Roest, W. R. (2000). Potential-field signatures of buried Precambrian basement in the Western Canada Sedimentary Basin. *Canadian Journal of Earth Sciences*, 37(11), 1453-1471.

Price, R. (1981). The Cordilleran foreland thrust and fold belt in the southern Canadian Rocky Mountains. *Geological Society, London, Special Publication*, *9*(1), 427-448.

Riazi, N., & Eaton, D. W. (2020). Anatomy of a buried thrust belt activated during hydraulic fracturing. *Tectonophysics*, 795, 228640.

Rohais, S., Crombez, V., Euzen, T. & Zonneveld, J.-P. (2018). Subssidence dynamics of the Montney Formation (Early Triassic, Western Canada Sedimentary Basin): insights for its geodynamic setting and wider implications. Bulletin of Canadian Petroleum Geology, 66, 128–160.

Romero-Sarmiento, M.F., Euzen, T., Rohais, S., Jiang, C., Littke, R., 2016. Artificial thermal maturation of source rocks at different thermal maturity levels: Application to the Triassic Montney and Doig formations in the Western Canada Sedimentary Basin. Org. Geochem. 97, 148–162. https://doi.org/10.1016/j.orggeochem.2016.05.002.

Richards, B. C., Barclay, J. E., Osadetz, K. G., Trollope, F. H., & Hartling, A. (1990). Carboniferous strata of the Western Canada sedimentary basin. Bulletin of Canadian Petroleum Geology, 38(1), 178-178.

Root, K. G. (2001). Devonian Antler fold and thrust belt and foreland basin development in the southern Canadian Cordillera: implications for the Western Canada Sedimentary Basin. *Bulletin of Canadian Petroleum Geology*, 49(1), 7-36.

Ross, G. M., Milkereit, B., Eaton, D., White, D., Kanasewich, E. R., & Burianyk, M. J. (1995). Paleoproterozoic collisional orogen beneath the western Canada sedimentary basin imaged by Lithoprobe crustal seismic-reflection data. *Geology*, 23(3), 195-199.

Ross, G. M., Parrish, R. R., Villeneuve, M. E., & Bowring, S. A. (1991). Geophysics and geochronology of the crystalline basement of the Alberta Basin, western Canada. *Canadian Journal of Earth Sciences*, 28(4), 512-522.

Schoenball, M., & Ellsworth, W. L. (2017). A systematic assessment of the spatiotemporal evolution of fault activation through induced seismicity in Oklahoma and southern Kansas. Journal of Geophysical Research: Solid Earth, 122(12), 10-189.

Schultz, R., Skoumal, R. J., Brudzinski, M. R., Eaton, D., Baptie, B., & Ellsworth, W. (2020). Hydraulic fracturing-induced seismicity. *Reviews of Geophysics*, 58(3), e2019RG000695.

Shaw, J. H., & Suppe, J. (1996). Earthquake hazards of active blind-thrust faults under the central Los Angeles basin, California. *Journal of Geophysical Research: Solid Earth*, 101(B4), 8623-8642.

Shaw, J. H., & Shearer, P. M. (1999). An elusive blind-thrust fault beneath metropolitan Los Angeles. *Science*, 283(5407), 1516-1518.

Sheriff, R. E. (1992). Vertical and lateral seismic resolution and attenuation: part 7. Geophysical methods.

Sikabonyi, L. A., & Rodgers, W. J. (1959). Paleozoic tectonics and sedimentation in the northern half of the West Canadian Basin. Bulletin of Canadian Petroleum Geology, 7(9), 193-216.

Skuce, A. G. (1996). Frontal Foothills structures in central Alberta: the thin end of the intercutaneous wedge?. Bulletin of Canadian Petroleum Geology, 44(2), 153-164.

Smith, D. A. (1980). Sealing and nonsealing faults in Louisiana Gulf Coast salt basin. *AAPG Bulletin*, 64(2), 145-172.

Spencer, C. W. (1987). Hydrocarbon generation as a mechanism for overpressuring in Rocky Mountain region. *AAPG Bulletin*, 71(4), 368-388.

Valkó, P. (2000). Hydraulic fracturing. Kirk-Othmer Encyclopedia of Chemical Technology, 1-24.

Vannoli, P., Basili, R., & Valensise, G. (2004). New geomorphic evidence for anticlinal growth driven by blind-thrust faulting along the northern Marche coastal belt (central Italy). *Journal of Seismology*, 8(3), 297-312.

Westgate, M., Manzi, M. S., Malehmir, A., Gibson, R. L., Andreoli, M. A., & Bumby, A. (2021). A reappraisal of legacy reflection seismic data from the western margin of the Kaapvaal craton, South Africa, with implications for Mesozoic-Cenozoic regional tectonics. Tectonophysics, 813, 228934.

Wolfe, F. D., Shaw, J. H., Plesch, A., Ponti, D. J., Dolan, J. F., & Legg, M. R. (2019). The Wilmington Blind-Thrust Fault: An Active Concealed Earthquake Source beneath Los Angeles, California. *Bulletin of the Seismological Society of America*, 109(5), 1890-1906.

Withjack, M. O., & Callaway, S. (2000). Active normal faulting beneath a salt layer: an experimental study of deformation patterns in the cover sequence. *AAPG Bulletin*, 84(5), 627-651.

Wood, J. M., Sanei, H., Haeri-Ardakani, O., Curtis, M. E., Akai, T., & Currie, C. (2018). Solid bitumen in the Montney Formation: Diagnostic petrographic characteristics and significance for hydrocarbon migration. International Journal of Coal Geology, 198, 48-62.

Wozniakowska, P., & Eaton, D. W. (2020). Machine Learning-Based Analysis of Geological Susceptibility to Induced Seismicity in the Montney Formation, Canada. Geophysical Research Letters, 47(22), e2020GL089651.

Wright, G. N., McMechan, M. E., Potter, D. E. G., Mossop, G. D., & Shetsen, I. (1994). Structure and architecture of the Western Canada sedimentary basin. Geological Atlas of the Western Canada Sedimentary Basin, 25-40.

Zonneveld, J.-P. & Moslow, T.F. (2018). Palaeogeogaphic setting, Lithostratigraphy, and sedimentary framework of the Lower Triassic Montney Formation of western Alberta and northeastern British Columbia. Bulletin of Canadian Petroleum Geology, 66, 93–127.

Appendix A

The Montney Formation is divided in to Lower, Middle and Upper Montney members characterized by the distinct depositional environments within each of the subunits which influenced the facies distribution. In this report, we use the subdivision into Lower, Middle and Upper Montney according to the literature sources introduced in *Geological Setting* section of the report, presented in the Fig. A1.

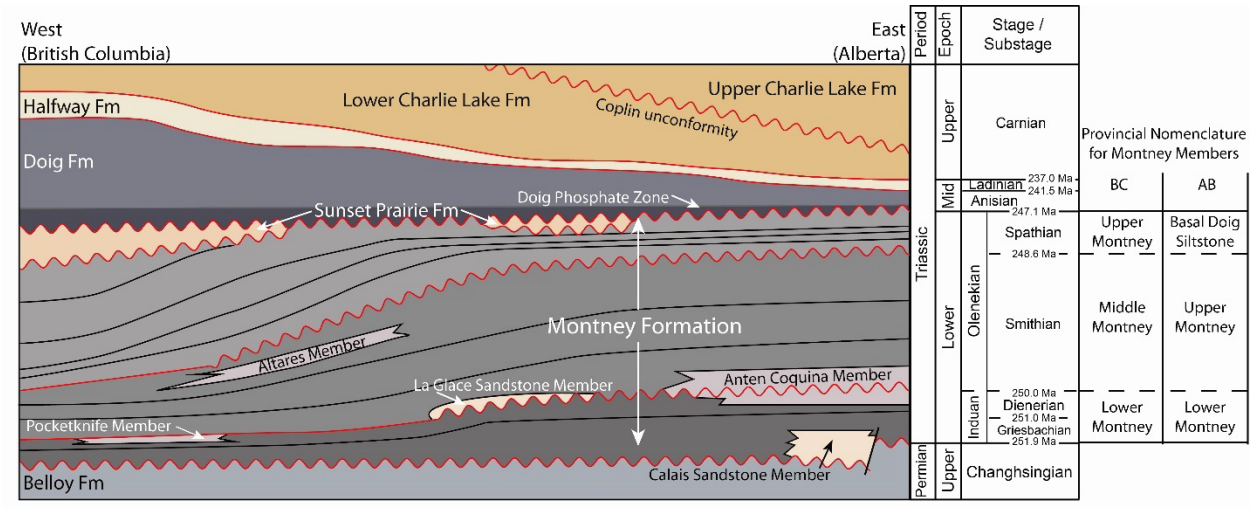

Fig. A1. Schematic west-east oriented cross section showing Montney stratigraphy in central Alberta to northeastern British Columbia. Three main Montney members (Lower, Middle and Upper) are highlighted, as well as other members and units that are lithologically different and locally isolated within the Montney. Modified from Zonneveld and Moslow (2018).

Seismic data –preprocessing

The next step of our analysis includedinterpretation of the seismic data within the area of study. In addition to publicly available LITHOPROBE seismic profiles, we have analyzed one seismic line located within one of the seismic monitoring regions. Originally provided seismic SEGY files contained incorrect values for the Easting and Northing coordinates assigned to the seismic traces, which required additional preprocessing to obtain the correct coordinate values.

Originally available SEGY files did not have correctly assigned coordinate values due to crooked geometry of the lithoprobe seismic lines (Fig. A2). As a result, seismic traces were not assigned to the correct location jn space, yielding poor-quality seismic images. To resolve this issue, original coordinate had to be updated before loading the SEGY files into the seismic interpretation software.

Analysis of the SEGY files revealed that seismic headers contain several sets of coordinates: source coordinates, group coordinates and coordinate values included in additional column, originally named “SourceDepth” named correct coordinate values can be retrieved from one of the seismic headers. Comparison of coordinates and geometry of the LITHOPROBE line 11A is presented in the Fig. A2. enlargement of the seismic line and plotting it as line charts allowed for more in-depth analysis of coordinate point sets and revealed, that updated coordinate values recalculated from differences in the point locations between the coordinate point sets recalculated from “SourceDepth” are placed in the correct order, as opposed to the rest of the coordinate collections which produced unordered line charts.

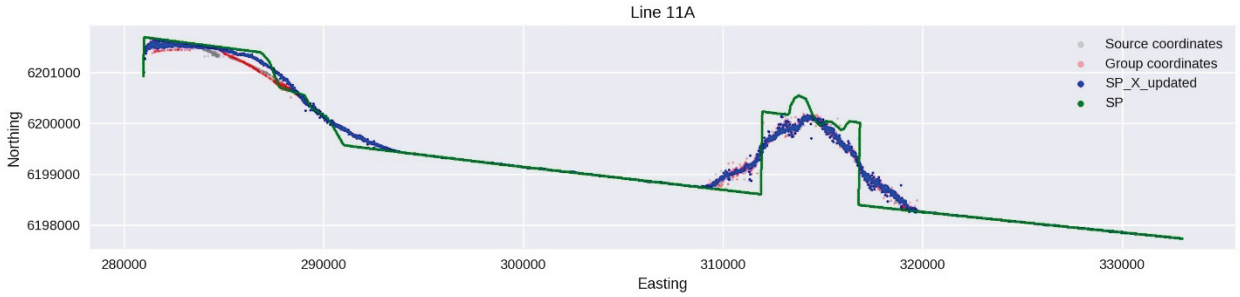

Fig. A2. Comparison of coordinates provided with seismic line 11a. Green points correspond to the shot point coordinates from the SEGP1 file. Grey and pink points correspond to source, group coordinates from the geometry SEGY file associated with line 11a. Blue points show the location of the shot point coordinates accessed through the trace headers, under alternative name column (originally named as "SourceDepth"). Source coordinates were changed to units of m (e.g., SourceDepth was provided in units of 100m).

In the last step, recalculated Easting coordinates were used to determine the updated Northing value for the points located on to the smoothed line, considered as an ideal approximation of the shot point locations along the seismic profile. Smoothed line was determined using Savitzky-Golay filter, which is a commonly used interpolation method of smoothing the data based on predefined number of points. In our calculation, we have compared three window sizes: 11, 31 and 51; Window size 51 was chosen as the best suited for our application, which was considered as the best approximation of the seismic line.

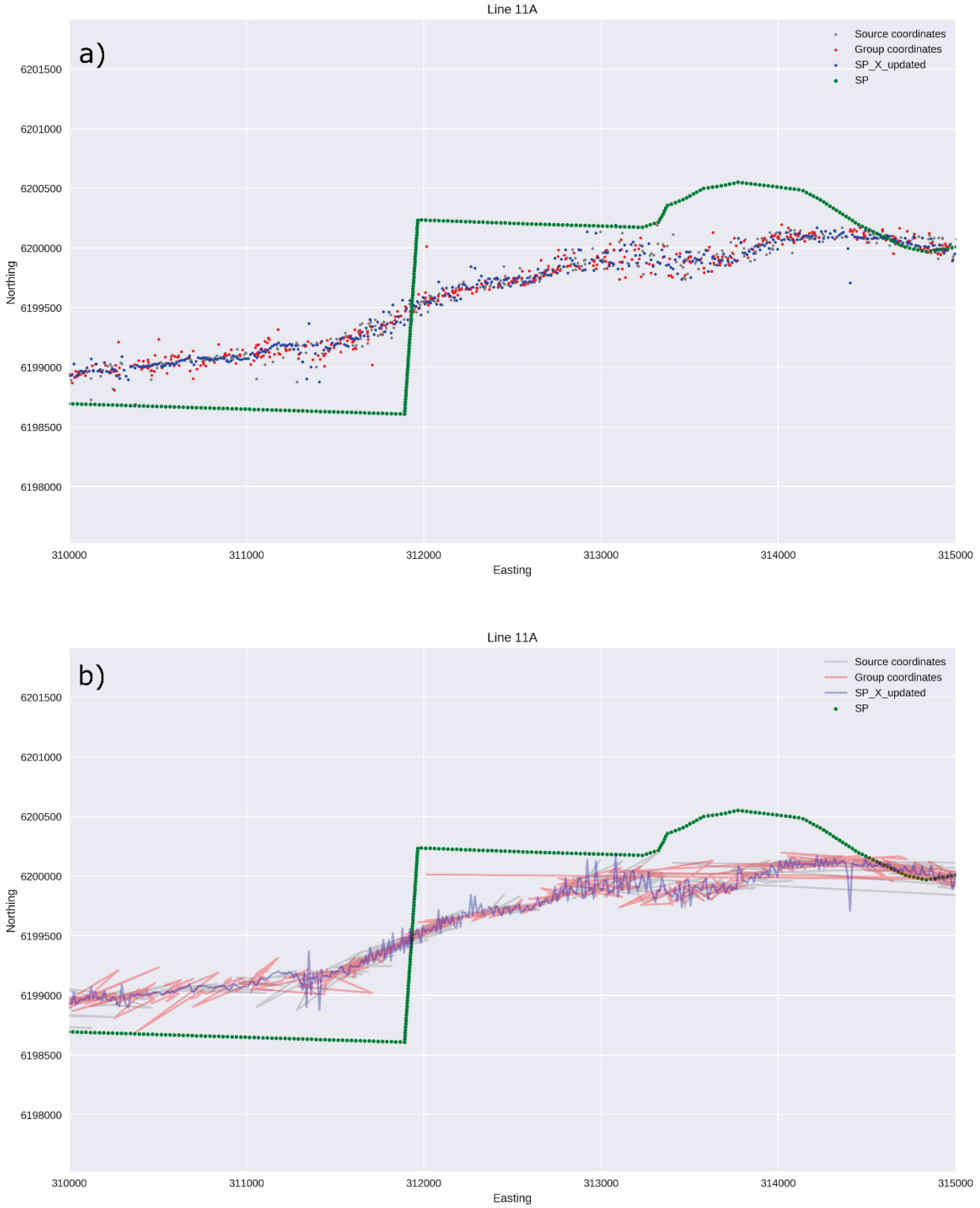

Fig. A3. Zoom into the scatter plot (a) and line plot (b) of the coordinate sets presented in the Fig. A1. Plots were limited by setting the limits on the Easting axis between 310000m and 315000 m. Source and Group coordinates, unlike updated Shotpoint coordinates seem to be not have correctly assigned values, which is indicated by the "chaotic" line charts. During interpolation of Y coordinates of the Shotpoints, coordinates indicated by the blue points in the Fig. A1b. were used.

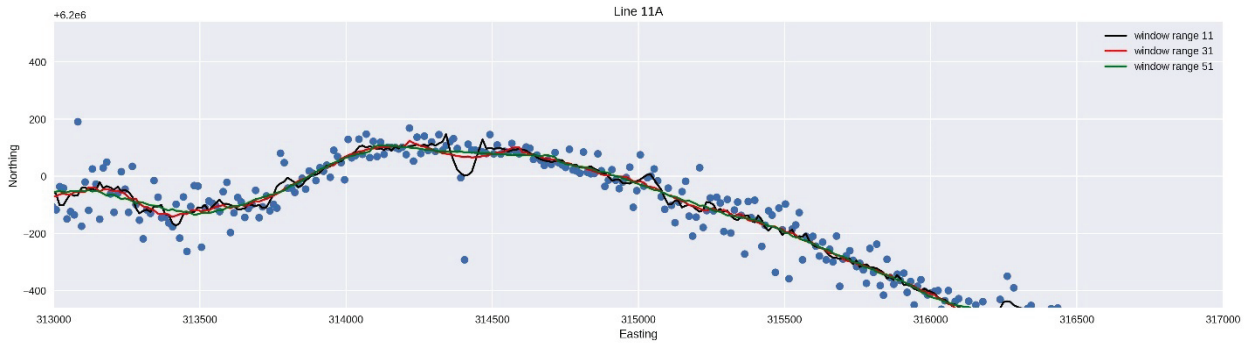

Fig. A4. Results of the interpolation using Savitzky-Golay filter using 3 different window ranges (11, 31, and 51). Window ranges indicate the number of datapoints used during interpolation over the running window. The window of size 51, which resulted in most smooth curve was used to determine the new Northing coordinates.

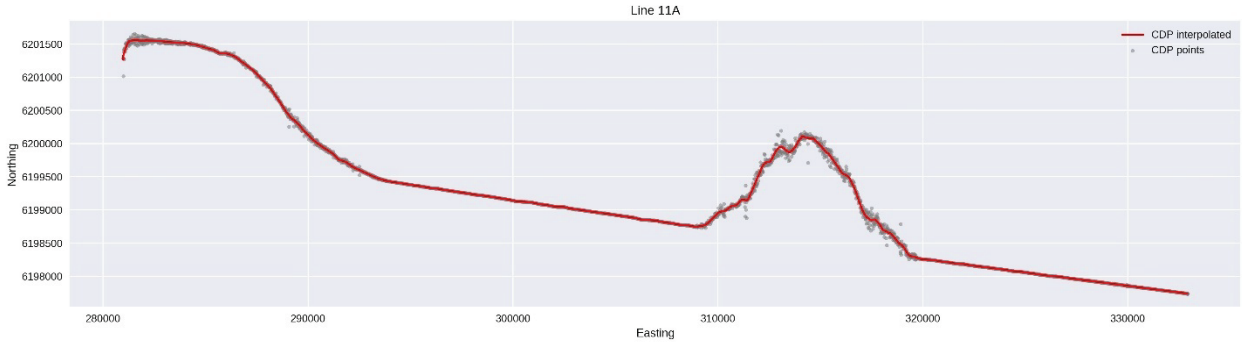

Fig. A5. Results of the interpolation using Savitzky-Golay filter using the filter window of size 51. Window ranges indicate the number of datapoint used to during the interpolation over the running window. The window of size 51, which resulted in most smooth curve was used to determine the new Northing coordinates.

<u>Geometric calculations from seismic data and residual maps.</u>

Apparent throw calculations

Apparent throw (h_{app}) estimation was performed for Wabamun formation since the clarity of expression for this horizon was continuous throughout all seismic profiles analyzed in this study. Calculation consisted of in two steps.

First, apparent depth difference (dz_{app}) was calculated using formula (1):

$$dz_{app} = 0.5 \times d_t \times V_{av} \quad (1)$$

where:

d_t - time difference corresponding to the shift on the Wabamun horizon (fault throw)
V_{av} - average seismic velocity in Wabamun (assumed to be 4500m/s)

In the next step, apparent throw (h_{app}) was determined according to formula (2):

$$h_{app} = dz_{app} / \cos(\text{fault dip}) \quad (2)$$

where:

dz_{app} – apparent throw calculated using formula (1)

Table. A1. Geometrical parameters of structural corridors estimated from seismic data. Primary uncertainties of the apparent throw correspond to the errors related to the average velocity estimation. To illustrate, 10% increase in the value of the average velocity results in 9% increase of the apparent throw value, which implies that the apparent throw calculation errors in meters increase proportionally and are therefore more noticeable for structures characterized by larger apparent throws.

	Gordondale L11a (West)	Gordondale L11b (East)	Rycroft L11b (West)	Dunvegan L12cd (East)	Dunvegan L12cd (East)	Tangent 12F (North-West)	Tangent L13 (South-East)
t1 [s]	1.90	1.93	1.85	1.77	1.65	1.71	1.51
t2 [s]	2.05	2.08	1.92	1.80	1.75	1.55	1.57
V_{av} [m/s]	4500	4500	4500	4500	4500	4500	4500
dip [deg]	37	35	42	30	21	41	45
dt [ms](abs)	0.15	0.06	0.07	0.03	0.11	0.16	0.06
dz_{app} [m]	338	144	157.50	68	239	362	131
h_{app} [m]	**194**	**335**	**107**	**58.4**	**222**	**273**	**92.2**

Apparent width calculations

Apparent width calculation is a suggested method to estimate the width of the structural corridors in the areas where information about the corridor geometry could not be inferred from seismic due to data unavailability. It is achieved by identifying the relationship between the width of the structural corridors intersected by seismic lines (including examples from literature) defined as the distance between 2 most distant faults included within the same corridor and length of the corridor estimated from the Residual maps. In addition to seismic data, we have investigated the literature examples of structural corridors to increase the number of observations to infer the geometrical trends.

Structural corridor width *w* was determined by using the trigonometric relationships between the angle between apparent width determined along the seismic profile *w'* and angle between the seismic line and strike of the corridor according φ to the formula:

$$w = w' \sin \varphi \quad (3)$$

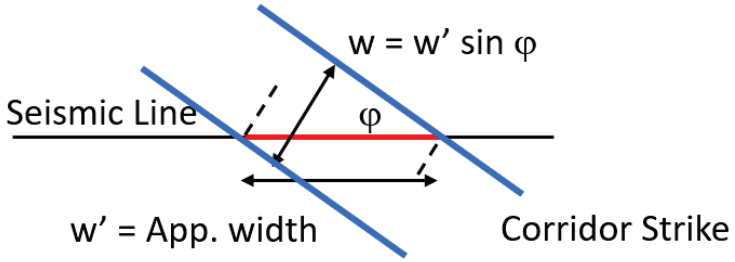

Fig. A6. Schematic of structural corridor width estimation using seismic data.

Table A2. Parameters of the structural corridors intersected by seismic profiles used to investigate geometric relationships between length and width of corridors are presented in the Tab. A1. Estimated corridor widths estimation include approximately 5% error which could correspond to incorrect corridor length or angle estimation.

	Length [km]	Apparent width [km]	Width [km]	Length/Width
Gordondale	87.5	66	14.7 ± 0.7	5.9
Rycroft	83.4	21	15.4 ± 0.8	5.4
Dunvegan	94.1	27	18.2 ± 0.9	5.2
Tangent	27.7	13	4.08 ± 0.2	6.8
Monias*	36.2	-	6.4 ± 0.3	6.1

*Monias structural corridor is estimated from the seismic image.

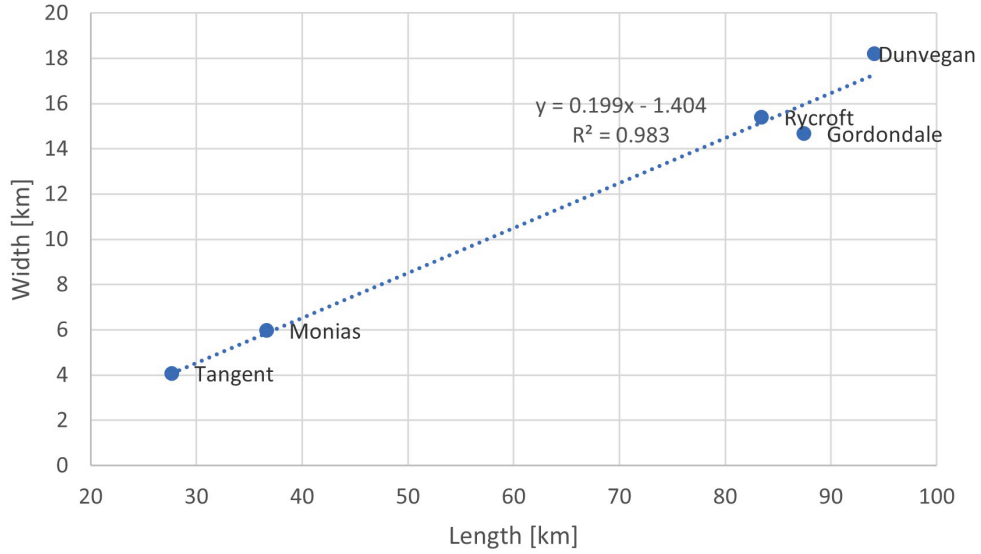

Fig. A7. Relationship between length and half width of the structural corridors. Linear trend is described by the equation 0.199x – 1.404, where x corresponds to the corridor length.

Estimation of width of the structural corridors identified using TSA

Empirical relationship was then used to investigate the relationship between length and width of the corridors for which seismic data was not available and length were determined using the residual maps. Using limited dataset it was observed that width of the structural corridors followed the generalized positive trend which can be approximated by the line represented by the formula below (4):

$$y = 0.199x - 1.404 \quad (4)$$

Where:

x – estimated length of the corridor

y – estimated width of the corridor

Estimation of vertical displacements of the structural corridors identified using TSA

Highest and lowest values of Wabamun, Debolt and Basal Fish Scale Zone (BFSZ) residuals within structural corridors intersected by the LITHOPROBE lines (Gordondale, Rycroft, Dunvegan and Tangent) were used to compare vertical displacements for each of the formations. Minimum (min), maximum (max), and vertical displacement (defined as the difference between minimum and maximum values) for each structural corridor were calculated using Image Analyst Toolbox included in ArcGIS Pro Software and are presented in the Table A3.

Values of the displacements are increasing with the age of the formations and for each structural corridor highest values are observed for Wabamun formations. Displacements within BSFZ are less significant. Comparing the displacements within structural corridors, Gordondale structural corridor is consistently characterized by the highest value of displacements for each residual, as compared to the Tangent structural corridor for which these values are few times smaller.

Table A3. Vertical displacements within Structural Corridors calculated from trend surface analysis (measured in meters).

	Gordondale	**Rycroft**	**Dunvegan**	**Tangent**
BFSZ min	-32.18	-20.07	-14.69	-9.35
BFSZ max	45.89	23.39	27.52	16.70
BFSZ range	**76.02**	**37.07**	**33.61**	**20.77**
Debolt min	-115.13	-62.96	-36.99	-21.78
Debolt max	76.96	59.86	66.45	40.30
Debolt range	**192.09**	**122.81**	**103.44**	**62.08**
Wabamun min	-123.23	-95.50	69.29	-39.86
Wabamun max	81.08	74.06	80.13	55.67
Wabamun range	**204.31**	**169.56**	**149.42**	**98.53**

Figures A8 to A14 show maps of the residual surfaces for the seven formations considered in this study, based on trend surface analysis.

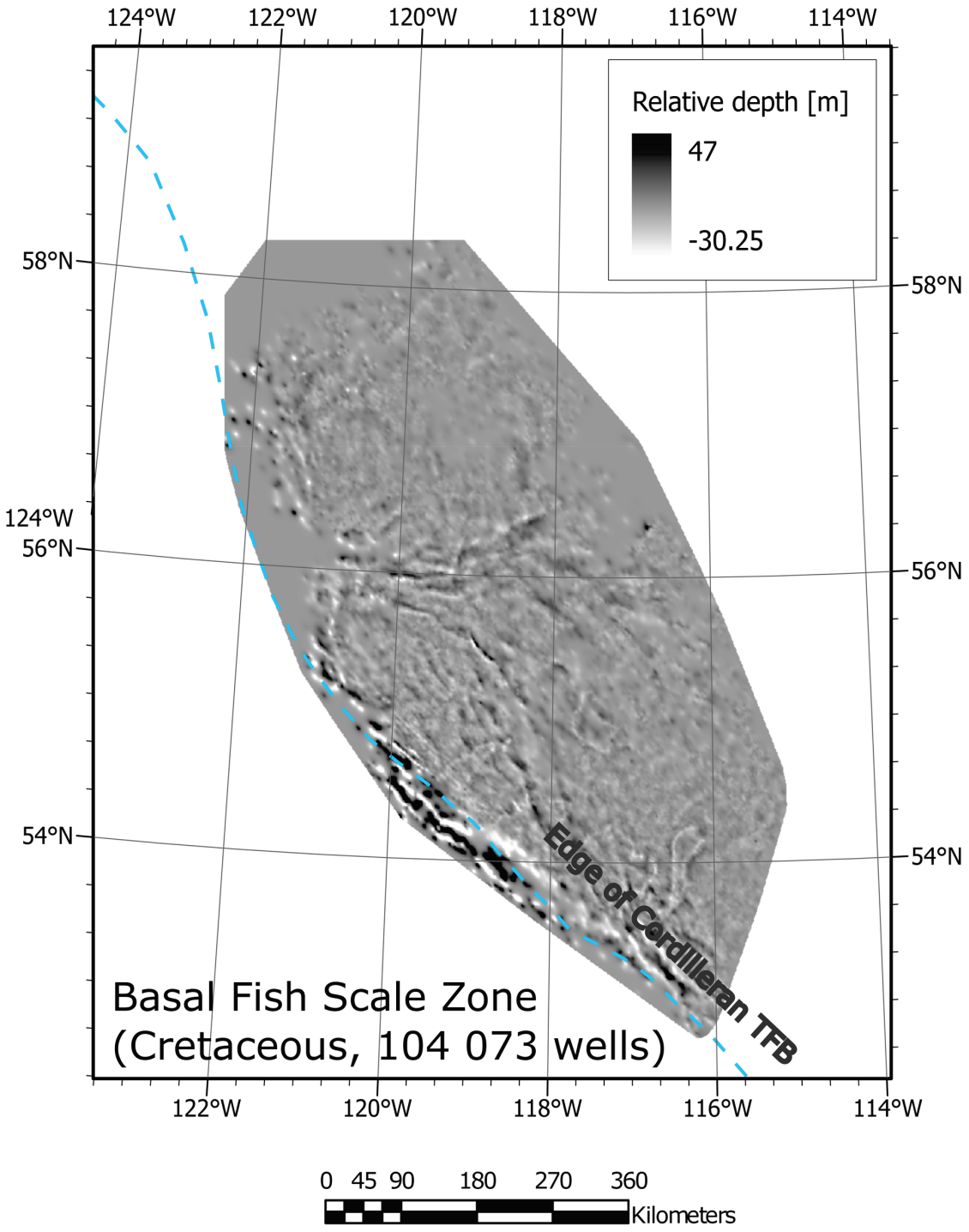

Fig. A8. Residual map of Basal Fish Scale Zone (BSFZ) top. Coherent trends in the maps are indicative of structural corridors (faults and folds). For reference, the eastern edge of the Cordilleran TFB is indicated by the dashed blue line. For each unit, the age and number of wells used for residual calculation are indicated in the lower left of the map.

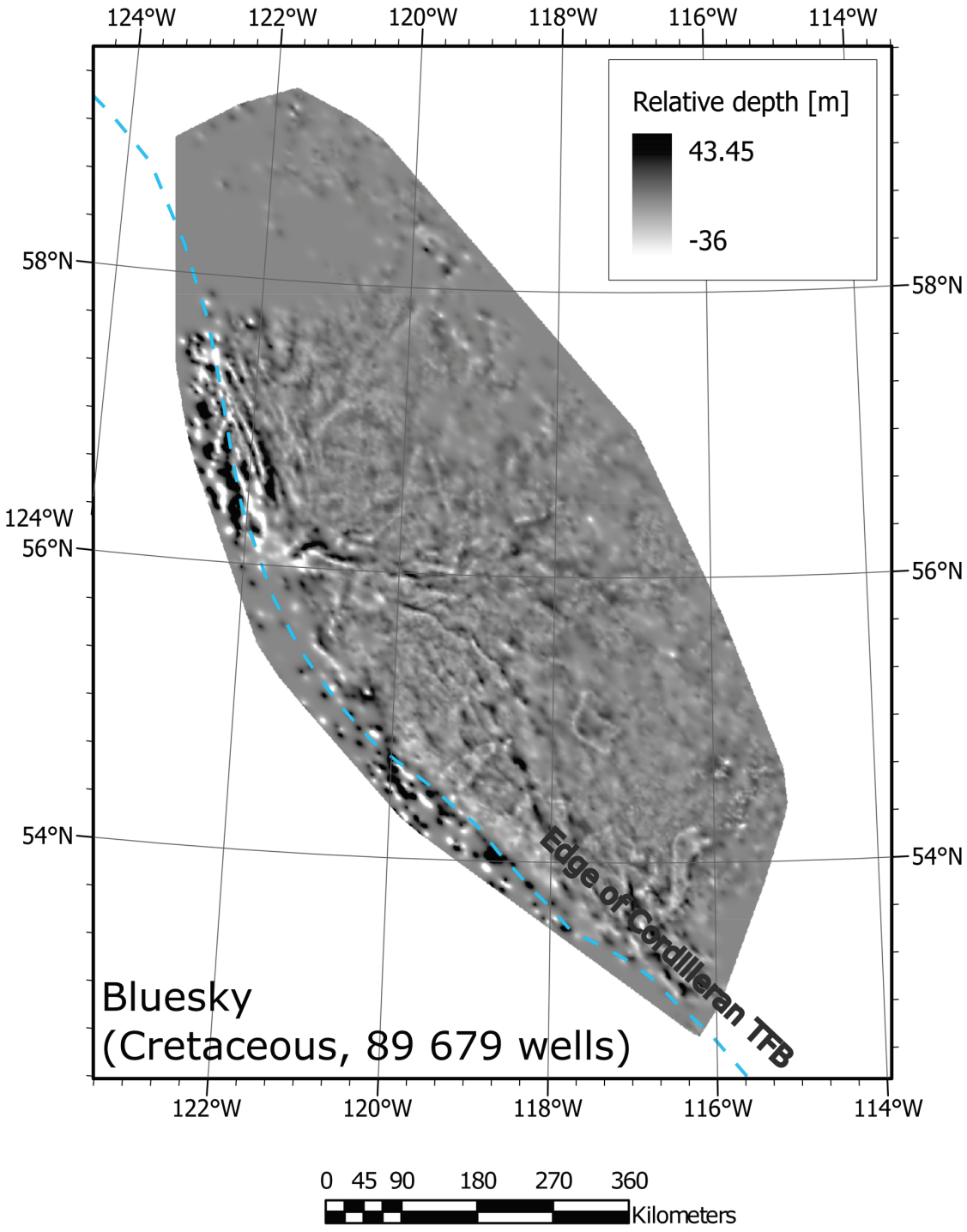

Fig. A9. Residual map of Bluesky top. Coherent trends in the maps are indicative of structural corridors (faults and folds). For reference, the eastern edge of the Cordilleran TFB is indicated by the dashed blue line. For each unit, the age and number of wells used for residual calculation are indicated in the lower left of the map.

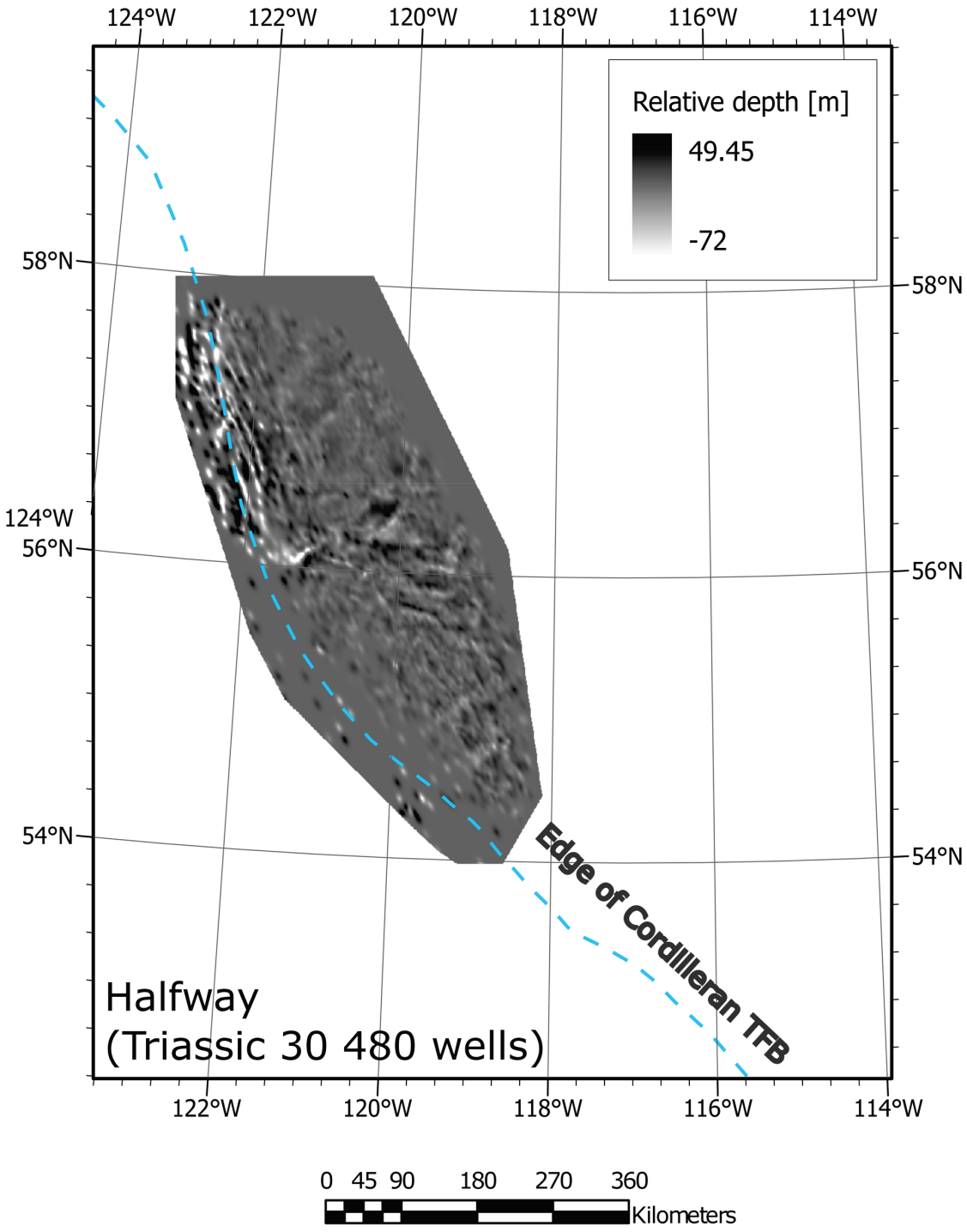

Fig. A10. Residual map of Halfway top. Coherent trends in the maps are indicative of structural corridors (faults and folds). For reference, the eastern edge of the Cordilleran TFB is indicated by the dashed blue line. For each unit, the age and number of wells used for residual calculation are indicated in the lower left of the map.

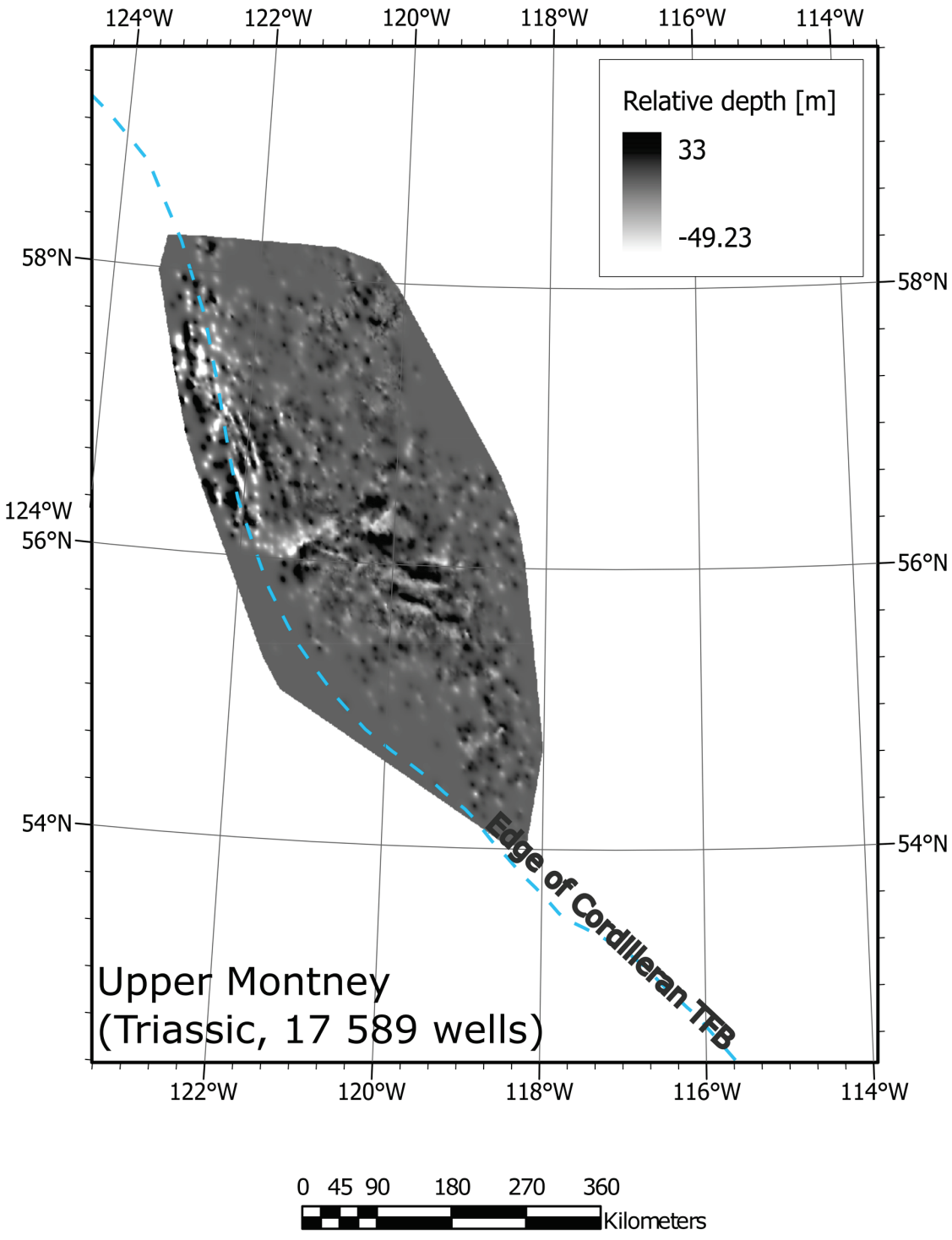

Fig. A11. Residual map of Upper Montney top. Coherent trends in the maps are indicative of structural corridors (faults and folds). For reference, the eastern edge of the Cordilleran TFB is indicated by the dashed blue line. For each unit, the age and number of wells used for residual calculation are indicated in the lower left of the map.

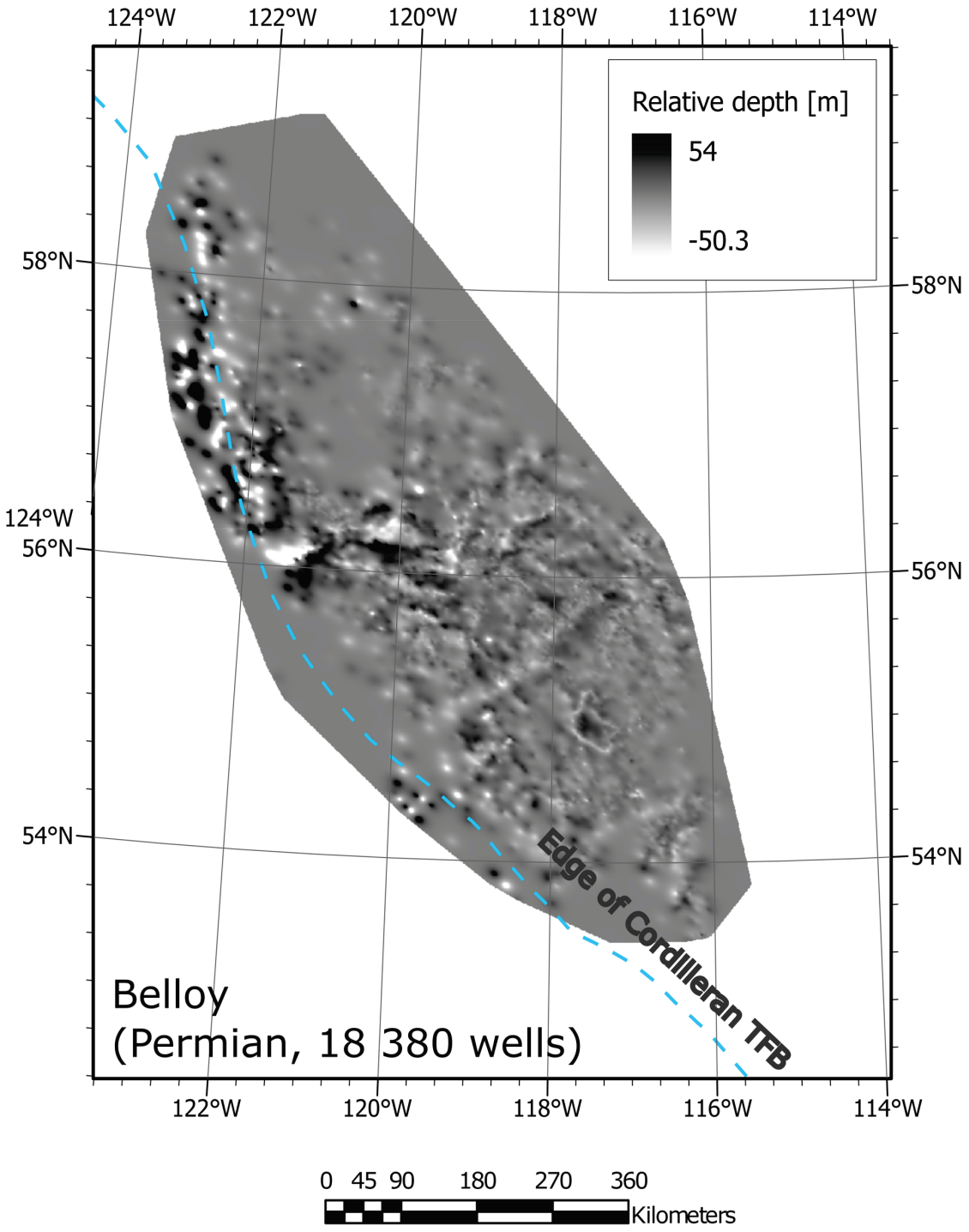

Fig. A12. Residual map of Debolt top. Coherent trends in the maps are indicative of structural corridors (faults and folds). For reference, the eastern edge of the Cordilleran TFB is indicated by the dashed blue line. For each unit, the age and number of wells used for residual calculation are indicated in the lower left of the map.

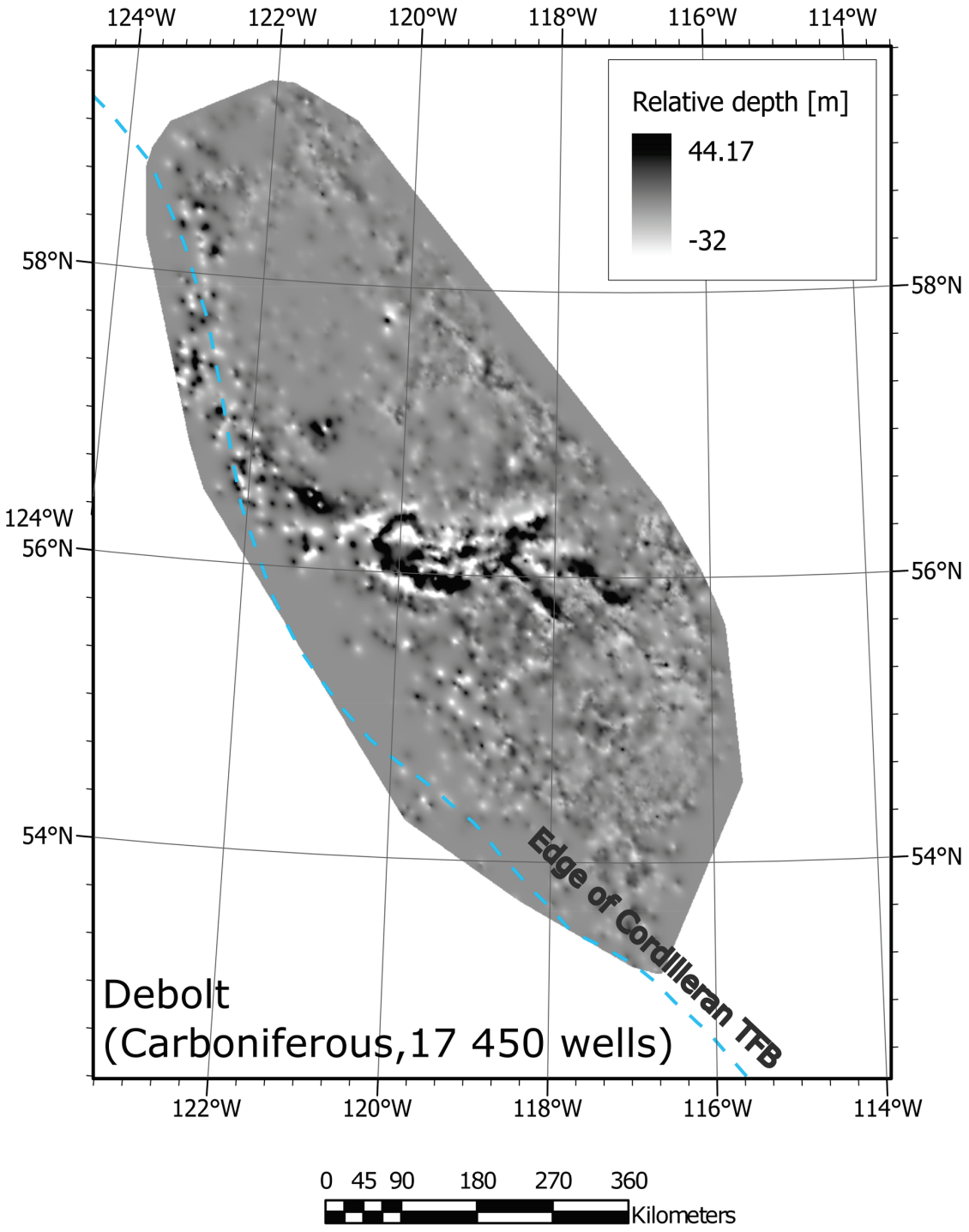

Fig. A13. Residual map of Debolt top. Coherent trends in the maps are indicative of structural corridors (faults and folds). For reference, the eastern edge of the Cordilleran TFB is indicated by the dashed blue line. For each unit, the age and number of wells used for residual calculation are indicated in the lower left of the map.

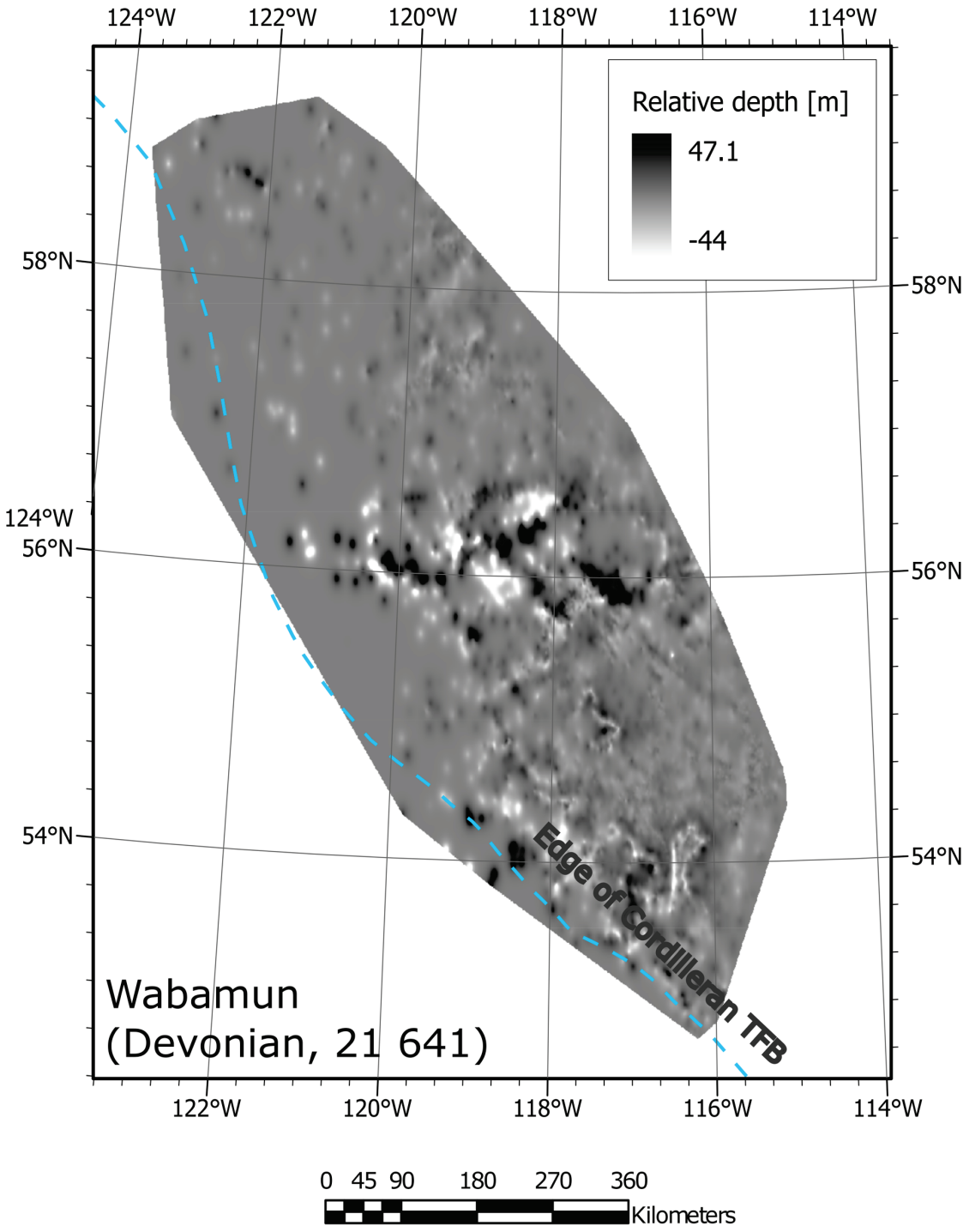

Fig. A14. Residual map of Wabamun top. Coherent trends in the maps are indicative of structural corridors (faults and folds). For reference, the eastern edge of the Cordilleran TFB is indicated by the dashed blue line. For each unit, the age and number of wells used for residual calculation are indicated in the lower left of the map.